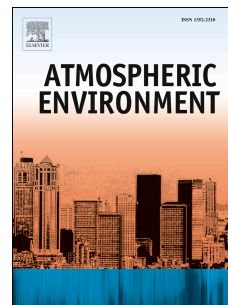


Accepted Manuscript

WRF-Chem model sensitivity to chemical mechanisms choice in reconstructing aerosol optical properties

A. Balzarini, G. Pirovano, L. Honzak, R. Žabkar, G. Curci, R. Forkel, M. Hirtl, R. San José, P. Tuccella, G.A. Grell



PII: S1352-2310(14)00981-9

DOI: [10.1016/j.atmosenv.2014.12.033](https://doi.org/10.1016/j.atmosenv.2014.12.033)

Reference: AEA 13483

To appear in: *Atmospheric Environment*

Received Date: 30 May 2014

Revised Date: 11 December 2014

Accepted Date: 13 December 2014

Please cite this article as: Balzarini, A., Pirovano, G., Honzak, L., Žabkar, R., Curci, G., Forkel, R., Hirtl, M., San José, R., Tuccella, P., Grell, G.A., WRF-Chem model sensitivity to chemical mechanisms choice in reconstructing aerosol optical properties, *Atmospheric Environment* (2015), doi: 10.1016/j.atmosenv.2014.12.033.

This is a PDF file of an unedited manuscript that has been accepted for publication. As a service to our customers we are providing this early version of the manuscript. The manuscript will undergo copyediting, typesetting, and review of the resulting proof before it is published in its final form. Please note that during the production process errors may be discovered which could affect the content, and all legal disclaimers that apply to the journal pertain.

1 WRF-Chem model sensitivity to chemical mechanisms choice 2 in reconstructing aerosol optical properties

3
4 A. Balzarini ^{a,*}, G. Pirovano ^a, L. Honzak ^b, R. Žabkar ^{b, c}, G. Curci ^d, R. Forkel ^e, M. Hirtl ^f, R. San José ^g, P. Tuccella ^d
5 and G. A. Grell ^h

6
7 ^a Ricerca sul Sistema Energetico (RSE S.p.A.), via Rubattino 54, Milano, Italy

8 ^b Center of Excellence "SPACE-SI", Aškerčeva 12, Ljubljana, Slovenia

9 ^c University of Ljubljana, Faculty of Mathematics and Physics, Jadranska 19, Ljubljana, Slovenia

10 ^d Department of Physical and Chemical Sciences, Center of Excellence for the forecast of Severe Weather (CETEMPS),
11 University of L'Aquila, L'Aquila, Italy

12 ^e Karlsruhe Institut für Technologie (KIT), IMK-IFU, Kreuzteckbahnstr. 19, 82467 Garmisch-Partenkirchen, Germany

13 ^f Zentralanstalt für Meteorologie und Geodynamik, ZAMG, Hohe Warte 38, 1190 Vienna, Austria

14 ^g Environmental Software and Modelling Group, Computer Science School - Technical University of Madrid, Campus
15 de Montegancedo - Boadilla del Monte-28660, Madrid, Spain

16 ^h NOAA Earth System Research Laboratory, Global System Division, 325 Broadway, Boulder, Colorado

17
18 * Corresponding author: Alessandra Balzarini

19 Phone: +39.02.3992.5286

20 Fax: +39.02.3992.4608

21 e-mail: alessandra.balzarini@rse-web.it

22 **Abstract:**

23 In the framework of the AQMEII initiative WRF-Chem has been applied over Europe adopting two chemical
24 configurations for the calendar year 2010. The first one employed the RADM2 gas-phase chemistry and
25 MADE/SORGAM aerosol module, while the second one implemented the CBM-Z gaseous parameterization and
26 MOSAIC aerosol chemistry. Configurations shared the same domain, meteorological setups and input data.

27
28 The Comparison demonstrated that CBM-Z has a more efficient ozone-NO titration than RADM2 in regions with
29 sufficiently high levels of NO_x and VOCs. At the same time, CBM-Z is found to have a more effective NO₂ + OH
30 reaction. The parameterization of the relative humidity of deliquescence point has a strong impact on HNO₃ and NO₃
31 concentrations over Europe, particularly over the sea. The MADE approach showed to be more efficient than MOSAIC.
32 Differently, particulate sulfate and SO₂ ground concentrations proved to be more influenced by the heterogeneous SO₂
33 cloud oxidation.

34 PM10 and PM2.5 have shown similar results for MOSAIC and MADE/SORGAM, even though some differences were
35 found in the dust and sea salt size partitioning between modes and bins. Indeed, in MADE the sea salt was distributed
36 only in the coarse fraction, while the dust emissions were distributed mainly in the fine fraction.

37 Finally, different chemical mechanisms give different Aerosol Optical Depths (AOD). WRF-Chem is found to under
38 predict the AODs in both configurations because of the misrepresentation of the dust coarse particle, as shown by the
39 analysis of the relationship between the Angström exponent and the AOD bias. Differently, when the AOD is

40 dominated by fine particles, the differences in model performance are more evident, with MADE/SORGAM generally
41 performing better than MOSAIC. Indeed the higher availability of both sulfate and nitrate has a significant influence on
42 reconstruction of the AOD estimations.

43 This paper shows the great importance of chemical mechanisms in both gaseous and aerosols predictions, as well as in
44 the calculation of aerosol optical properties.

45

46 **Research Highlights:**

- 47 • CBMZ-MOSAIC and RADM2-MADE/SORGAM chemical mechanisms were compared within WRF-Chem
- 48 • CBM-Z is more accurate than RADM2 in reconstructing the gaseous species
- 49 • MADE shows better performances than MOSAIC for PM
- 50 • Optical properties reflects the skill of mechanisms in reproducing aerosol compounds
- 51 • Weaknesses and strengths of both mechanisms were pointed out and discussed

52

53 **Keywords:** CBMZ-MOSAIC, RADM2-MADE/SORGAM, online coupled model, model inter-comparison, chemical
54 mechanism, optical properties

55

56 **1 Introduction**

57 Different chemical mechanisms may lead to dissimilar aerosol predictions. Recent air quality modeling studies show
58 large uncertainties in aerosol treatments (Solazzo et al., 2012), causing significant discrepancies in the simulation of
59 ground concentrations and optical features.

60 However, previous modeling inter-comparison studies were largely conducted with offline models (Cuvelier et al.,
61 2007; Rao et al., 2011; Pernigotti et al., 2013; Van Loon et al., 2007). Moreover, in all these studies model performance
62 evaluation (MPE) has been widely based on the comparison of modeled concentration of the aerosol bulk mass and
63 main chemical compound (Pirovano et al., 2012; Kondragunta et al., 2008), while less consideration has been devoted
64 to the evaluation of model performance in reproducing aerosol optical properties. Only few studies analyzed the aerosol
65 optical properties over Europe (Basart et al., 2012; Robles González et al., 2003), mainly using off-line models;
66 whereas some example of on-line coupled models were applied over the US (Zhang et al. 2012; Chapman et al., 2009).

67 Online coupled meteorology and chemistry models are becoming more and more popular in air quality modeling
68 applications as they enable to achieve a significant reduction of inconsistency between meteorological and chemical
69 processes as well as taking into account the influence of feedback effects, mainly related to aerosol load (Baklanov et
70 al., 2014; Grell and Baklanov, 2011; Zhang et al., 2010). In order to increase knowledge on them the second phase of
71 the Air Quality Model Evaluation International Initiative (AQMEII <http://aqmeii.jrc.ec.europa.eu/>) was focused on
72 online coupled meteorology-chemistry models.

73 In this study, a coupled on-line modeling system, the Weather Research and Forecasting Model (Skamarock et al. 2008)
74 coupled with Chemistry (WRF-Chem; Grell et al., 2005) was used to investigate the influence of different chemical
75 mechanisms on aerosol concentrations and to analyze the relationship between the outcome of the traditional MPE and
76 the aerosol optical properties.

77 In WRF-Chem the chemistry transport and transformations are embedded into WRF so that the interactions between
78 meteorology and the chemistry can be investigated (Grell et al., 2005).

79 In the frame of the second phase of the AQMEII initiative (Alapaty et al., 2012), the WRF-Chem model has been
80 applied over Europe for the calendar year 2010, adopting two different chemical configurations.

81 In contrast to previous studies (Cuvelier et al., 2007; Rao et al., 2011; Pernigotti et al., 2013; Pirovano et al., 2012; Van
82 Loon et al., 2007), the present application focused also on analyzing the on-line model sensitivity to chemical
83 mechanisms in reproducing AODs; therefore enabling comprehensive conclusions on the influence of model chemical
84 formulation on the modeled aerosol properties.

85 To this aim, a thorough evaluation and comparison of the model results has been performed. Traditional MPE has been
86 employed comparing ground level observed data with both pollutants collected at the European Airbase sites
87 (<http://acm.eionet.europa.eu/databases/airbase/>) and PM composition data provided by the EMEP network (European
88 Monitoring and Evaluation Programme; <http://www.emep.int/>). Additionally, the model's ability in reproducing aerosol
89 optical properties (AODs), relevant for feedback effects, has been investigated using AERONET (Aerosol Robotic
90 Network; <http://aeronet.gsfc.nasa.gov/>) observed data.

91 The following section (Section 2) describes the main features of the model and the modeling configurations adopted in
92 the study. In Section 3 a detailed analysis of model results is presented. Only aerosols species and their main precursors
93 are considered in the analysis because of their key role on feedback effects. Finally, Section 4 discusses the main
94 finding and conclusions.

95

96 **2 Model set up**

97 WRF-Chem (version3.4.1, August 2012) has been used to investigate the modeling sensitivities of two different
98 combinations of chemical mechanisms and aerosol modules. The first one is denoted with SI2 and includes the RADM2
99 (Second Generation Regional Acid Deposition Model; Stockwell et al. 1990) gas phase mechanism, the
100 MADE/SORGAM (Modal Aerosol Dynamics Model for Europe/Secondary Organic Aerosol Model; Ackermann et al.,
101 1998 and Schell et al., 2001) aerosol module for secondary inorganic (SIA) and organic aerosols (SOA); whereas CBM-
102 Z (Carbon Bond Mechanism version Z; Zaveri and Peters, 1999) and MOSAIC (Model for Simulating Aerosol
103 Interactions and Chemistry ; Zaveri et al.,2008) modules have been selected for the IT1 simulation.

104 RADM2 is a condensed gas-phase photooxidation mechanism that was developed by Stockwell et al. (1990). It uses a
105 “lumped molecule” technique in which similar organic compounds are grouped together in different model categories
106 (Middleton et al., 1990; Grell et al., 2005). RADM-2 includes 63 chemical species and 136 gas-phase reactions.

107 The MADE module, used in the first configuration. is a modal scheme that describes three log-normally distributed
108 modes to simulate particle size distribution: the Aitken mode ($< 0.1 \mu\text{m}$ diameter), the accumulation mode ($0.1 - 2 \mu\text{m}$
109 diameter), and the coarse mode ($> 2 \mu\text{m}$ diameter). In each mode particles are assumed to have the same chemical
110 composition (internally mixed), while they are externally mixed among different modes (Zhao et al., 2010).

111 In the CBM-Z mechanism the inorganic chemistry is based on Gery et al. (1989) and Stockwell et al. (1990) with
112 modified photolytic rate constants as described in DeMore et al. (1997). Organics are treated with a “lumped structure”
113 approach where a set of model species are used to represent different parts of the molecule as if they reacted
114 independently. It contains 52 prognostics species and 132 gas-phase reactions.

115 The MOSAIC module treats the gas to particle partitioning and the thermodynamic equilibrium for sulfate, nitrate,
116 ammonium, sodium, calcium, chloride, and water. In this work the 4-bin version of the mechanism is selected ($0.04 -$
117 $0.156 \mu\text{m}$; $0.156 - 0.625 \mu\text{m}$; $0.625 - 2.5 \mu\text{m}$; $2.5 - 10 \mu\text{m}$). The current implementation of MOSAIC does not account
118 for the secondary organic aerosol processes.

119 Simulations adopted the same simple wet deposition module for grid-resolved precipitation, based on Grell and Freitas
120 (2014). This approach was also accounted in SI2 run for the calculation of the wet removal processes for non-resolved
121 convective precipitation. On the contrary, simulations included the same Wesely (1989) dry deposition approach. The

122 photolysis frequencies have been calculated with the Fast-J scheme (Barnard et al., 2004) under clear and cloudy sky
123 conditions in both simulations. However, the heterogeneous cloud oxidation of SO₂ is included only in SI2 run. In
124 particular, SI2 included the CMAQ (Community Multiscale Air Quality Model; Byun and Ching, 1999; Byun and
125 Schere, 2006) aqueous phase chemistry in the convective parameterization (Walcek and Taylor, 1986) and the
126 GOCART (Goddard Chemistry Aerosol Radiation and Transport) SO₂ to SO₄ conversion for grid-scale precipitation.
127 In WRF-Chem the aerosol optical properties (e.g. extinction coefficient, single-scattering albedo, and the asymmetry
128 factor) are computed as a function of wavelength over the vertical dimension (Fast et al., 2006; Zhao et al., 2010). Each
129 aerosol chemical component is associated to a complex index of refraction. The overall refractive index for a given size
130 bin (or mode) is determined by volume averaging and then used to calculate aerosol optical properties based on the Mie
131 theory (Zhao et al., 2010) adopting the methodology described by Ghan et al. (2001). A detailed explanation of the
132 aerosol optical properties computation can be found in Barnard et al. (2010).

133 The Aerosol Optical Depth (AOD) is defined as the integral of the extinction coefficient over the atmosphere, therefore
134 it was calculated as a sum along each vertical profile of the product of the extinction coefficients computed by WRF-
135 Chem by the corresponding layer thickness. Before performing the vertical integration, WRF-Chem extinction
136 coefficients have been interpolated to the AERONET wavelengths (470, 555 and 675 nm) following the Angström law
137 (Tombette et al., 2008).

138 Model configurations shared the same physical parameterizations, namely the Noah Land Surface Model (Chen and
139 Dudhia, 2001), Morrison double-moment microphysics scheme (Morrison et al., 2009), RRTMG long-wave and
140 shortwave radiation schemes (Rapid Radiative Transfer Model for Global; Iacono et al., 2008), Grell 3D ensemble
141 cumulus parameterization (Grell and Devenyi, 2002), Yonsei University Planetary Boundary Layer (YSU; Hong et al.,
142 2006) and Monin-Obukov surface layer.

143 WRF-Chem has been applied for the whole year of 2010 covering Europe and a portion of Africa as well as large areas
144 affected by the Russian forest fires. The domain (Figure 1) is defined in a Lambert Conic Conformal projection that
145 includes 270 x 225 grid points with 23 km of horizontal resolution. The vertical grid extends over 33 stretched layers
146 from the surface to a fixed pressure of 50 hPa (about 20 km), with the lowest level thickness of 24 m close to the
147 ground.

148 As required by the exercise, model runs have been integrated over individual 2-day periods. Each run also included a
149 meteorological spin up time of one day prepared using the meteorological WRF model with identical physical options.
150 Chemical fields at the end of a 2-day simulation have been, then, passed on as initial fields for the following simulation.
151 Models have been driven by the input data set provided in the framework of the exercise, including the TNO-MACC
152 (<http://www.gmes-atmosphere.eu>; Kuenen et al., 2014, Pouliot et al., 2012) anthropogenic emissions, the Finnish
153 Meteorological Institute (FMI) inventory for biomass burning emissions (<http://is4fires.fmi.fi>), the ECMWF IFS-
154 MOZART chemical boundary conditions and the ECMWF operational archive fields. More details on the input data are
155 provided in Pouliot et al. (2014), Brunner et al. (2014) and Forkel et al. (2014).

156 Natural emissions have been calculated on-line. Biogenic emissions were computed using the MEGAN model (version
157 2.04, Guenther et al., 2006). Sea salt emissions were based on wind speed at 10 m (Gong et al., 2003), whereas dust
158 emission calculation applied the Shaw et al. (2008) algorithm adjusted for the tunable proportionality constant and for
159 desert dust spurious fluxes.

160

161 **3 Results and discussion**

162 Results have been compared to observations by means of the ENSEMBLE system (<http://ensemble2.jrc.ec.europa.eu/>),
163 a web-based platform for the inter-comparison and evaluation of atmospheric chemistry transport models (Bianconi et
164 al., 2004; Galmarini et al., 2012).

165 Ground-based observations from Airbase and EMEP networks have been provided for the year 2010. Only rural
166 background stations have been considered in the analysis, since they are the most adequate for comparing model results
167 over a 23km-grid resolution. Furthermore, only stations that had more than 75% of data availability have been included.
168 A set of 497 sites were found to fulfill the selection criteria for hourly O₃, while hourly SO₂ and NO₂ were available
169 from 224 and 366 monitoring stations, respectively. Daily data from 306 sites have been collected for PM₁₀. Surface
170 observations for daily PM_{2.5} have been provided by 105 stations. Ground observations from 34 sites have been used for
171 sulfate, while 14 and 19 stations have been analyzed for nitrate and ammonium, respectively. Fine total organic carbon
172 measurements were available only at Ispra site (Italy; IT0004R).

173 Aerosol Optical Depths at the wavelength of 555 nm and Angström exponent at the wavelength of 440-675 nm have
174 been also considered from twelve AERONET stations, whose geographical characteristics and data availability is
175 reported in Table S1 (auxiliary material).

176 Model performance has been evaluated using the following statistical parameters: Modeled Mean, Observed Mean,
177 Pearson's Correlation Coefficient (PCC), Normalized Mean Bias (NMB) and Root Mean Square Error (RMSE). For a
178 complete definition of these indices refer to Appendix A.

179 A detailed performance evaluation of the current meteorological setups has been discussed in Brunner et al. (2014).
180 However, box-whisker plots of the statistical indices for temperature, mixing ratio and wind speed are made available in
181 the auxiliary material. Figure S1 reveals that configurations show comparable results for the main meteorological
182 parameters over Europe.

183

184 3.1 Gaseous species

185 Figure 2 shows the spatial distribution of yearly mean concentrations of gas phase compounds that lead to Secondary
186 Inorganic Aerosols (SIA) for the two configurations. IT1 and SI2 reveal a quite coherent behavior in reconstructing the
187 spatial plot of gaseous species, but some differences can be depicted close to the main emissive sources. O₃
188 concentrations from RADM2 are generally 2-6 ppb higher than those for CBM-Z over the North of Europe and along
189 the ship tracks in the Mediterranean and the North Atlantic Ocean (Figure2a).

190 The pattern of the difference in near surface ozone is mostly associated with changes in NO₂ concentrations (Figure 2b).
191 IT1 simulation shows a slightly positive bias of NO₂ concentrations (0.4-0.6 ppb) over the high emissive areas of
192 Europe and along the international shipping routes. This occurs because O₃ and NO₂ concentrations are strongly
193 influenced by local scale effects, such as the ozone-NO titration (Pirovano et al., 2012). CBM-Z seems to reveal more
194 efficient ozone-NO titration than RADM2 in regions with sufficiently high levels of NO_x and VOCs. However, in some
195 urban areas (e.g. Paris, London, Milan, etc.) SI2 has higher ozone yearly mean concentrations with respect to IT1 (IT1 =
196 15-20 ppb, SI2 = 25-30 ppb), even though the NO₂ concentrations are generally high (IT1 = 12-14 ppb, SI2 = 14-20
197 ppb). This can be attributed to the RADM2 chemistry solver implemented in WRF-Chem. Forkel et al. (2014) found
198 that the currently used configuration adopted a QSSA-like solver that underrepresents the ozone-NO titration in regions
199 with high NO emissions. As a result, in urban environments an enhanced near surface O₃ concentration can be
200 estimated.

201 SO₂ yearly mean concentrations are 0.1-0.5 ppb higher in IT1 than SI2 (Figure 2c), although they show the same spatial
202 distribution over Europe. The highest values are located in the Eastern European countries where the surface level
203 sources of SO₂ are still relevant and along the international shipping routes (1.6-2 ppb).

204 SO₂ is a primary compound mainly emitted from aloft sources. Both configurations share the same anthropogenic
205 emissions and the same vertical distribution for point source emissions, suggesting that the differences may be
206 associated to the reconstruction of SO₂ oxidation processes within the model. As discussed by Aan de Brugh et al.
207 (2011) chemical oxidation has a strong impact on SO₂ ground concentrations, and the presence of the heterogeneous
208 SO₂ cloud oxidation is found to favor the formation of particulate sulfate in SI2 (Figure 5a). Therefore, reduced SO₂
209 concentrations at the ground can be likely expected for SI2. In order to further confirm this assumption, the distribution
210 of H₂O₂ was analyzed, being one of the most efficient oxidant of sulfuric compounds in clouds and fogs (Senifeld and
211 Pandis, 1998). As can be seen in Figure 2d, IT1 has also the highest concentrations of H₂O₂, showing differences of
212 0.04-0.2 ppb with respect to SI2 and thus indicating an inefficient SO₂ aqueous oxidation to sulfate.

213 IT1 generally predicts higher HNO₃ concentrations than SI2 over Europe (Figure 2e).. The largest differences in HNO₃
214 concentrations are found along the shoreline and the main ship tracks over the Mediterranean Sea and the Atlantic
215 Ocean, where simulations can vary up to 0.80 ppb. The differences in HNO₃ predictions can be partially related to the
216 different reaction rates constants in the photochemical reaction of NO₂ with OH. At a temperature of 300°K, the
217 reaction rate constant for NO₂ + OH + M → HNO₃ is about 1.3 times higher in CBM-Z than in RADM2. Moreover, the
218 two simulations have different treatment of the gas-to-particle partitioning from nitric acid to ammonium nitrate as a
219 function of relative humidity. MADE adopted the Mozurkewich (1993) approach, while the Zaveri et al. (2008) method
220 is applied in MOSAIC. As discussed lately, MADE shows a more efficient thermodynamic treatment of the equilibrium
221 between nitric acid and ammonium nitrate especially for those areas characterized by relative humidity higher than the
222 deliquescence point. The highest reaction rate constants and the different treatment of the gas-to-particle partitioning
223 may produce the highest HNO₃ mixing ratios in CBM-Z.

224 Since the importance of removal process as a sink for gaseous HNO₃, an analysis of HNO₃ dry deposition has been
225 conducted over the whole year 2010. Unfortunately, a detailed investigation of deposition fields cannot be done for the
226 present study since there were not measurements data, and simulated results were only available for SI2. Therefore dry
227 deposition can only be evaluated by comparing SI2 model results to other WRF-Chem simulations performed into the
228 AQMEII exercise. DE4 and ES3 were chosen for the analysis. DE4 configuration is similar to SI2, while ES3 uses the
229 same options as IT1, but with feedback effects turned on. For more detail on DE4 and ES3 simulations refer to Forkel et
230 al. (2014) and San José et al. (2014), respectively. As it can be seen in Figure S2, HNO₃ dry deposition is comparable
231 among the three runs, even though ES3 generally shows lower values than SI2 and DE4. This is consistent with the
232 previous findings that exhibited greater HNO₃ concentrations for IT1.

233 Table 1 presents the comparison among observed and modeled gaseous concentrations in all rural background stations.
234 The time series of modeled and observed daily concentrations are shown in Figure 3. Both runs underestimate the
235 gaseous yearly mean concentrations. However, CBM-Z generally performs better for SO₂ and NO₂, while RADM2 has
236 better performances in terms of O₃. Simulated SO₂ has a Normalized Mean Bias of -41.64% (IT1) and -45.62% (SI2),
237 because of an under prediction occurring during the whole year (Figure 3c). NO₂ is underestimated by -36.74% (IT1)
238 and 39.88% (SI2). Large model errors are found in correspondence of winter months when the highest NO₂
239 concentrations are observed (Figure 3b). The general underestimation of modeled NO₂ and SO₂ may be partly attributed
240 to biases in meteorological variables, including an overestimation of surface wind speed of about 30% (Brunner et al.,

241 2014). This may lead to too strong dilution of air pollutants thus contributing to the under prediction of primary air
242 compounds (Brunner et al., 2014).

243 Ozone shows lower NMB that ranges from -3.75% (SI2) to -12.32% (IT1). As a consequence of NO₂ underestimation,
244 simulations tend to underestimate ozone concentrations from January to August, whereas the September-December
245 period is well captured by the model. Furthermore, configurations simulate reasonably well the shape of the ozone day-
246 to-day variation (Figure 3a). Indeed, they present a noticeable skill in terms of correlation. IT1 shows a value of 0.82,
247 while SI2 has a correlation score of 0.85.

248

249 3.2 Aerosol compounds

250 As can be seen from the comparison of PM₁₀ and PM_{2.5} from SI2 and IT1 (Figure 4a and Figure 4b), simulations show
251 similar results over land, but they behave differently over the Saharan region and over the sea. Dust seems to be
252 partitioned differently for MADE and MOSAIC in the modified Shaw et al. (2008) dust module; although PM₁₀ dust is
253 higher for IT1 (up to 40 µg/m³), there is less PM_{2.5} dust as compared to SI2 (- 10 µg/m³). These results are consistent
254 with other WRF-Chem modeling studies. Zhao et al. (2010) reported that using the same dust emission scheme the
255 modal approach simulates up to 25% higher mass concentrations for fine dust particles and lower mass concentrations
256 (8%) for coarse dust particles than the sectional approach.

257 The sea salt in PM₁₀ and PM_{2.5} is different for MADE and MOSAIC. The huge PM_{2.5} difference between IT1 and
258 SI2 over the North Atlantic can be attributed to the fact that for MADE the sea salt is only distribute in the coarse
259 fraction. As a consequence PM_{2.5} concentrations of MOSAIC are up to 10 µg/m³ higher than MADE in the Atlantic
260 Ocean, even though MADE simulates major concentrations along the international shipping routes of the
261 Mediterranean. These model differences can be clearly explained by analyzing the SIA pattern (Figure 5).
262 Different sea salt size distribution between MADE and MOSAIC may have an impact on the aerosol-radiation
263 interactions. Since small particles scatter light most efficiently than coarse particles (Seinfeld and Pandis, 1998),
264 variations in global solar radiation can be expected between MADE and MOSAIC over the Atlantic Ocean when
265 aerosol direct effects are included.

266 Figures 5a – 5c depict SO₄, NO₃ and NH₄ concentrations for both simulations. SO₄ yearly mean concentrations are
267 always lower for IT1 than for SI2 (Figure 5a). As discussed previously, one of the most probable reasons of this bias is
268 that IT1 does not include the aqueous phase oxidation of sulfur dioxide (SO₂) by hydrogen peroxide (H₂O₂). The
269 finding seems to be confirmed also by Figure 6a, where the sulfate yearly time series of daily mean values is compared
270 to observed concentrations. IT1 under predicts particulate sulfate by a factor of 2 in winter, when the heterogeneous
271 sulfate formation by cloud oxidation of sulfur dioxide is predominant; whereas there is a closer agreement between
272 model (IT1) and observations during the summer month when sulfate is mainly derived via homogeneous nucleation of
273 gas-phase sulfuric acid produced by sulfur dioxide oxidation in presence of OH. On the contrary, SI2 shows a quite
274 homogeneous behavior during the whole year, though overestimating the SO₄ observed concentrations.. Consequently,
275 SI2 performances are generally better than IT1 (Table 1). Modeled SO₄ presents a positive bias in SI2 (NMB =
276 20.67%), while SO₄ is biased negative in IT1 (NMB = -47.02%). A possible reason of SI2 overestimation is the
277 underrepresentation of the in-cloud and below-cloud scavenging by precipitation of soluble PM_{2.5} species such as SO₄.
278 Under predictions of the monthly accumulated precipitations were identified by Brunner et al. (2014) especially in
279 winter months, and in western and eastern Europe where the main SO₄ variations between the two simulations are
280 found. Im et al. (2014) performed a collective analysis of models performance for aerosol compounds grouping data in
281 three different regions (western continental Europe, eastern continental Europe and Mediterranean area). The analysis

282 states that SI2 performances for SO₄ are very similar over the whole domain, while IT1 results are largely
283 underestimated over continental Europe (Mean Fractional Bias larger than 75%) whereas over the Mediterranean region
284 Mean Fractional Bias (MFB) is around -10%. Such a discrepancy can be related to the greater influence of aqueous-
285 phase oxidation of SO₂ in continental Europe with respect to the southern regions. These results seem to be in contrast
286 with Zhang et al. (2012) that compared CBM-Z mechanism with CB05 (Yarwood et al., 2005) and SAPRAC-99
287 (<http://www.cert.ucr.edu/~carter/absts.htm>) over the US. Their work showed an over prediction of sulfate with CBM-Z,
288 which gave also the highest concentrations of SO₄ among the three mechanisms due primarily to the domination of the
289 gas-phase oxidation of SO₂ by OH over the aqueous-phase oxidation by dissolved oxidants such as H₂O₂. However, the
290 simulation of Zhang et al. (2012) included the feedback effects, thus the Carnegie Mellon University (CMU)
291 mechanism of Fahey and Pandis (2001) was activated for the aqueous-phase chemistry. McKeen et al. (2007) and
292 Tuccella et al. (2012) found that models that embed the cloud aqueous-phase oxidation of sulfur dioxide overestimate
293 the ground concentrations of SO₄. Moreover, Aan de Brugh et al. (2011) assessed that 45% of SO₂ aqueous-phase
294 oxidation to sulfate over Europe happens within the planetary boundary layer, thus it may have a significant
295 contribution on surface concentrations of both SO₂ and SO₄. These results suggest that the introduction of the aqueous-
296 phase oxidation of sulfur dioxide in the standard CBM-Z/MOSAIC option would be highly required for a better
297 reconstruction of the sulfate concentrations at the ground, especially during winter months.

298 NO₃ concentration in the atmosphere is determined by the concentration of its main precursor HNO₃ and the
299 thermodynamic equilibrium between HNO₃ and nitrate. As shown in Figure 5b, NO₃ reveals different behavior with
300 respect to SO₄. Simulations expose a quite coherent pattern over land, while the main differences are related to the sea-
301 land interface. Over the sea, where relative humidity is generally higher than deliquescence point, the gas-to-particle
302 partitioning from nitric acid to ammonium nitrate seems to be more efficient in MADE than in MOSAIC. In particular,
303 the Mozurkewich (1993) approach adopted in MADE appears more effective than the Zaveri et al. (2008) available in
304 MOSAIC, thus, determining higher NO₃ concentrations over the Mediterranean Sea. On the contrary over Europe,
305 where EMEP stations are located, NO₃ concentrations are 0.4-1 µg/m³ higher for MOSAIC than for MADE/SORGAM
306 (Figure 5b), according to the highest availability of HNO₃ mixing ratios. All simulations over predict NO₃
307 concentrations in all seasons (Figure 6b). The simulated NO₃ shows a very high positive bias in both simulations with a
308 NMB that ranges from 31.84% in IT1 to 114.82% in SI2 (Table 1). Similar results were obtained by Zhang et al. (2012)
309 over the US. They found an overestimation of NO₃ concentrations for CBM-Z with a NMB that ranges between 39.6%
310 and 245%. Moreover, Im et al. (2014) have shown that the largest NO₃ over prediction for both simulations occurs at
311 eastern and southern Europe (MFB > 150%), while the lowest overestimation take place over western Europe (MFB <
312 50%). This overestimation can be partly attributed to low simulated temperatures that favor the gas-phase nitric acid
313 (HNO₃) and ammonia (NH₃) conversion to particulate ammonium nitrate (NH₄NO₃) with respect to (NH₄)₂SO₄
314 (Brunner et al., 2014).

315 As a consequence of sulfate and nitrate overestimations, ammonium is biased high in both simulations (IT1 NMB =
316 31.84%; SI2 NMB = 114.82%), even though IT1 simulates lower yearly mean concentrations than SI2 (Table 1 and
317 Figure 5c). For both models the largest overestimation takes place in Southern Europe (Im et al., 2014), due to a
318 corresponding overestimation of nitrate and sulfate, particularly during the summer season.

319 Finally yearly mean concentrations of elemental carbon (EC) and organic carbon (OC) are reported in Figure 5d and
320 Figure 5e, respectively. Discrepancies between the two simulations are 0.3 µg/m³ for EC and 1 µg/m³ for OC, with
321 concentrations generally somewhat higher in the IT1 run. Considering that the two configurations shared the same
322 emission inventories, adopted a common treatment of vertical dispersion, and use the same dry deposition equation, the

323 differences should be caused by the different treatment of the aerosol dynamics, and dissimilar assumptions in
324 distributing the computed concentrations between modes and bins. This is quite relevant in the high-emissive areas of
325 Eastern Europe where different model assumptions can have a greater impact on model results.
326 Table 1 provides a comparison of model performance against Airbase and EMEP observations. WRF-Chem under
327 predicts PM10 and PM2.5 concentrations, but MADE/SORGAM generally performs better than MOSAIC. Modeled
328 PM10 shows a Normalized Mean Bias that ranges from -25.82% (IT1) to -22.94 (SI2), while PM2.5 shows a NMB of -
329 14.05% and -11.76% for IT1 and SI2, respectively. Im et al. (2014) illustrated that the largest PM2.5 underestimation
330 for all models and all European regions takes place during the winter season (MFB larger than 50%). Differently,
331 during the summer season PM2.5 concentrations are partially overestimated by both models over both western and
332 eastern Europe, while still underestimated at Mediterranean sites. As previously detailed, summer overestimation, larger
333 for SI2 than IT1, is probably related to a corresponding overestimation of SIA. Conversely, PM underestimation is
334 connected to the reconstruction of the carbonaceous species, particularly OC simulations are almost one order of
335 magnitude lower than the surface concentrations at the EMEP station of Ispra (IT0004R; not shown). Measurements
336 show a yearly mean value at IT0004R of $7.08 \mu\text{g}/\text{m}^3$ while models generally range between $1.05 \mu\text{g}/\text{m}^3$ (SI2) and 1.10
337 $\mu\text{g}/\text{m}^3$ (IT1). It is worth nothing that SI2 includes the SOA formation. However, the SORGAM representation of this
338 process inside the model seems to have only a minor impact on the simulated total fine concentrations of organic
339 carbon. Indeed, RADM2-MADE/SORGAM does not include the oxidation of biogenic monoterpenes and it has only a
340 partial treatment of anthropogenic VOC oxidation (McKeen et al., 2007; Tuccella et al., 2012).

341

342 *3.3 Optical properties*

343 Figure 7 shows the spatial pattern of yearly mean modeled AOD at 555nm of wavelength (AOD555), overlaid with
344 available observations from AERONET network. The highest simulated AOD555 values are observed in Northern
345 Europe whereas Mediterranean regions show lower values for both simulations. Discrepancies of about 70-80% are
346 found between IT1 and SI2 in the North Atlantic Ocean, indicating the important role of fine sea salt on the AOD
347 estimations. Particles between 0.1 and 1.0 μm diameter have higher scatter efficiency than coarse particles (Seinfeld
348 and Pandis, 1998), consequently larger amount of fine sea salt in IT1 can cause higher AODs. The magnitude of the
349 differences between the two simulation is less pronounced over the European continent, although some high values are
350 evident over center and north Europe, where differences between simulations can reach up 10-50%. On the contrary, in
351 southern Europe, where most AERONET sites are placed, IT1 is generally 20-30% lower than SI2.

352 The time series of simulated and observed daily mean AOD555 at all AERONET sites is represented in Figure 8,
353 whereas the corresponding performance statistics are given in Table 2. It is worth nothing that all AERONET stations
354 are located in the Mediterranean area, that is frequently subject to wind-blown dust episodes (Kallos et al., 2007;
355 Mitsakou et al., 2008).

356 Temporal variability between predicted and observed AOD555 is similar and well captured by both runs, with a
357 correlation ranging from 0.51 (IT1) to 0.52 (SI2). However, it usually over predicts the lowest observed values and it
358 misses a few hot spots of the measured trend. Daily mean AODs at all AERONET stations are spread between 0.03 and
359 0.4 whereas WRF-Chem has only few data points with AODs greater than 0.25. SI2 generally simulates higher values
360 than IT1. In fact, the predicted mean AOD555 is 0.12 and 0.14 for IT1 and SI2, respectively. As a consequence, IT1
361 shows a Normalized Mean Bias of -21.49%, while SI2 is biased lower (NMB = -6.39%).

362 Seinfeld and Pandis (1998) mentioned that fine ammonium nitrate and ammonium sulfate scatter light most efficiently
363 at the wavelength of 550 nm, suggesting that the large differences between IT1 and SI2 can be partly explained by the

364 different aerosol composition. Indeed at Southern European sites SI2 overestimated all SIA, while IT1 overestimated
365 nitrate and ammonium, and underestimated sulfate (Im et al., 2014). These findings are also consistent with Roy et al.
366 (2007) showing that sulfate dominates the total AOD in the Eastern United States with a relative contribution that can
367 reach up to 60%, while the combined OC and EC contributes only to 15%.

368 A specific analysis was carried out at Lampedusa (Italy) and Malaga (Spain). The sites were selected because the two
369 model configurations show opposite performance (Table 2 and Figure 9). Particularly, IT1 underestimates the observed
370 AODs (NMB in Lampedusa = -9.35; NMB in Malaga = -21.02); whereas SI2 over predicts them (NMB in Lampedusa
371 = 13.08; NMB in Malaga = 5.92). The scatterplots of AOD555 daily differences between the two models versus the
372 corresponding differences in daily fine nitrate and sulfate (Figure 10), computed for the whole year 2010, point out a
373 relationship between differences in SIA and AOD555. Correlation is close to 0.4 for sulfate in both stations, while the
374 agreement is better when nitrate biases are considered, which show a correlation of 0.59 and 0.60 in Lampedusa and
375 Malaga respectively. This is also evident analyzing Figure S3 in the auxiliary material. In Malaga the July-September
376 periods is characterized by some high spikes in simulated SI2 AODs that are less pronounced in IT1. These spikes
377 correspond in time with the difference between IT1 and SI2 for sulfate and nitrate concentrations, confirming that both
378 compounds are relevant in AOD555 estimations over Europe. As a consequence, the major availability of nitrate and
379 sulfate at the ground seems to determine higher AODs values in SI2 than IT1. These results are in line with Basart et al.
380 (2012) and Robles González (2003) that identified in SIA the main contributors to AOD values in the European
381 continent.

382 However, even though SIA are generally overestimated by the model, simulated AOD555 is biased negative in many
383 AERONET stations. In order to understand the reasons of model underestimations, time series of Cyprus and Nes Ziona
384 (Israel) are analyzed in Figure 11. In both stations model is found to under predict the measurements (Table 2). NMB
385 ranges from -30.03 (IT1) to -24.85 (SI2) in Cyprus, while Nes Ziona shows a NMB of -37.61 in IT1 and -31.79 in SI2.
386 AODs are analyzed together with the Angström exponent in the 400-600 nm wavelength interval that can be considered
387 an indicator of the particle distribution (Roy et al., 2007). Values that range between 1 and 2 indicate small particles
388 dominated by the accumulation mode; values nearly zero are indices of the presence of coarse aerosols (Eck et al.,
389 1999). The two model configurations show a good correlation with observations (Figure 11), although they do not
390 perform very well when coarse particle size dominates the pollution episodes over Southern Europe, as it is proved by
391 the Angström coefficient. As it can be seen in Figure 12, when the Angström exponent is high, there is a good
392 agreement between configurations and observations. On the contrary, deficiencies between model and observations
393 increase for low values of the Angström coefficient. In particular, if we take a closer look to Nes Ziona station, that is
394 typical of coarse-mode desert aerosols (Papadimas et al., 2008), the role of the dust component on the model skills is
395 remarkable. Conversely, in Cyprus air quality is strongly influenced by both local and transported pollution (Achilleos
396 et al., 2014) thus the effect of the dust component is still evident, but less pronounced. These results suggest that
397 AOD555 under prediction is mainly due to the misrepresentation of the dust coarse-mode particles, and that the dust
398 transport of coarse aerosols is still poorly reproduced by the model with the chosen dust option, even though some
399 corrections were introduced in the simulations.

400

401 **4 Conclusions**

402 Two WRF-Chem chemical modeling configurations have been applied in the framework of the AQMEII exercise in
403 order to investigate the influence of different chemical mechanisms on the reconstruction of both ground concentrations
404 and optical properties. The first configuration adopted the RADM2 gas-phase chemistry and MADE/SORGAM aerosol

405 reactions scheme, while the second one includes the CBM-Z gas-phase mechanism and the MOSAIC aerosol module.
406 Simulations shared exactly the same meteorological configurations as well as the same input data. However, only the
407 RADM2-MADE/SORGAM run included the heterogeneous cloud oxidation of SO₂. WRF-Chem has been applied over
408 Europe with 23 km of horizontal resolution for the whole year of 2010. Results were compared against observations by
409 means of the ENSEMBLE system.

410 Comparisons reveal that RADM2 calculates higher ozone and lower NO₂ surface concentrations than CBM-Z, because
411 of the less efficient ozone-NO titration in regions with sufficiently high levels of NO_x and VOCs. However, some
412 criticisms were identified in urban areas where RADM2 shows elevated ozone and NO₂ yearly mean concentrations.
413 This can be partially related to the RADM-solver implemented in WRF-Chem that tends to underestimate the ozone-
414 NO titration in urban environments as well as other regions with high NO emissions. Furthermore, differences in
415 conversion rate constants from NO₂ + OH to HNO₃ is found to be a strong source of uncertainties on HNO₃ estimations.
416 In particular, the highest rate constant of CBM-Z produces the highest HNO₃ concentrations over land. The HNO₃
417 pattern over Europe was also related to the different reconstruction of the gas-to-particle partitioning, which is found to
418 influence both gaseous and aerosol estimations. In particular, the treatment of the relative humidity of deliquescence in
419 the thermodynamic equilibrium is found to determine different gas-to-particle partitioning from nitric acid to
420 ammonium nitrate over the sea. The Mozurkewich (1993) approach adopted in MADE reveals to be more effective than
421 the Zaveri et al. (2008) in MOSAIC. As a consequence, MADE simulates lower HNO₃ concentrations and higher NO₃
422 concentrations than MOSAIC over the Mediterranean Sea. Moreover, results suggest that the heterogeneous SO₂ cloud
423 oxidation is the main player in the determination of particulate sulfate and SO₂ concentrations. The simulation
424 (RADM2-MADE/SORGAM) that included the aqueous-phase oxidation of SO₂ produced more realistic sulfate yearly
425 time series, even though the conversion from gas-to-particle of sulfur species is found to be too fast, thus,
426 overestimating sulfate and under predicting SO₂ concentrations at the ground.

427 PM₁₀ and PM_{2.5} of MOSAIC and MADE/SORGAM show similar results over the land, but they behave differently
428 over the Saharan region and over the sea. Dust and sea salt are partitioned differently for MADE and MOSAIC. Indeed,
429 in MADE the sea salt is only distributed into the coarse fraction. On the contrary the dust emissions seem distributed
430 mainly in the fine fraction for the dust option chosen. Since fine and coarse aerosols scatter light differently, dissimilar
431 particle size distribution of dust and sea salt concentrations between MADE and MOSAIC can have an impact on
432 aerosol-radiation interactions. Further investigations are necessary whether different chemical mechanisms may also
433 affect indirect effects.

434 As shown in this study, different chemical mechanisms give different AODs. WRF-Chem is found to under predict the
435 AOD₅₅₅ in both configurations because of the misrepresentation of the dust coarse particle transport within the model
436 over Mediterranean regions. Indeed, the analysis of the relationship between the Angström exponent and the AOD₅₅₅
437 bias, revealed that worst model performance take place more frequently during episodes dominated by the coarse
438 aerosol fraction.

439 Differently, when the AOD₅₅₅ is dominated by fine particles, the differences in model performance between the two
440 configurations are more evident, with MADE/SORGAM generally performing better than MOSAIC. Indeed the higher
441 availability of both sulfate and nitrate has a significant influence on reconstruction of the AOD₅₅₅ estimations.
442 The results obtained in this study show that the chemical mechanisms choice in is still a crucial aspect in modeling
443 estimations, even when on-line coupled models are concerned. Different WRF-Chem chemical mechanisms were found
444 to perform differently for gaseous and aerosol predictions. The importance of these results indicates a need for an
445 accurate representation of chemical components and reactions in order to obtain a correct reconstruction of aerosol

446 optical properties, particularly when trying to study aerosol direct and indirect effects. This applies for both natural and
 447 anthropogenic compounds. The former play a major role in the coarse aerosol fraction, but they can contribute also to
 448 the aerosol fine fraction, particularly in remote areas. As a consequence, a revision of the treatment and the assumptions
 449 concerning the dust and sea salt aerosol size distribution are highly recommended. Differently, in more urbanized areas
 450 the presence of fine particles, such as SIA, is mostly driven by anthropogenic sources.

451 Particularly, the study pointed out that both gas phase transformation pathways as well as heterogeneous processes can
 452 influence the atmospheric fate of nitrate and, as a consequence, its contribution to aerosol optical properties.

453 This study also demonstrated that the introduction of the aqueous-phase oxidation in the standard CBM-Z/MOSAIC
 454 option would be desirable for a better reconstruction of the ground sulfate concentrations. Finally, the study pointed out
 455 the need of using a more complex mechanisms for the treatment of SOA than the standard WRF-Chem options, such as
 456 the recently added Volatility Basis Set (VBS; Ahmadov et al., 2012).

457

458 **Acknowledgement**

459 We gratefully acknowledge the contribution of various groups to the second air Quality Model Evaluation international
 460 Initiative (AQMEII) activity: TNO (anthropogenic emissions database); ECMWF/MACC project & Météo-
 461 France/CNRM-GAME (chemical boundary conditions), FMI (fire emissions). Joint Research Center Ispra/Institute for
 462 Environment and Sustainability provided its ENSEMBLE system for model output harmonization and analyses, and
 463 evaluation. The RSE contribution has been financed by the Research Fund for the Italian Electrical System under the
 464 Contract Agreement between RSE S.p.A. and the Ministry of Economic Development - General Directorate for Nuclear
 465 Energy, Renewable Energy and Energy Efficiency in compliance with the Decree of March 8, 2006. The Centre of
 466 Excellence for Space Sciences and Technologies SPACE-SI is an operation partly financed by the European Union,
 467 European Regional Development Fund and Republic of Slovenia, Ministry of Higher Education, Science, Sport and
 468 Culture.

469

470 **Appendix A**

471 The statistical indicators selected to evaluate the model performances have been defined as follows:

472 Normalized Mean Bias (NMB):

$$473 \quad NMB = \frac{\sum_{i=1}^N (P_i - O_i)}{\sum_{i=1}^N O_i} \times 100$$

474 Root Mean Square Error (RMSE):

$$475 \quad RMSE = \sqrt{\frac{1}{N} \sum_{i=1}^N (P_i - O_i)^2}$$

476 Pearson's Correlation (PCC):

$$477 \quad PCC = \left[\frac{\frac{1}{N} \sum_{i=1}^N (O_i - \bar{O})(P_i - \bar{P})}{\sigma_O \sigma_P} \right]$$

478 P is the predicted concentration; O is the observed concentration and N is the number of pairs.

479

480 **References**

- 481 Aan de Brugh, J. M. J., Schaap, M., Vignati, E., Dentener, F., Kahnert, F., Soviev, M., Huijnen, V., Krol, M. C., 2011.
482 The European aerosol budget in 2006. *Atmos. Chem. Phys.*, 11, 1117–1139.
- 483
- 484 Achilleos, S., Evans, J.S., Yiallourous, P.K., Kleanthous, S., Schwart, J., Koutrakis, P., 2014. PM10 concentration levels
485 at an urban and background site in Cyprus: The impact of urban sources and dust storms. *Journal of the Air & Waste*
486 *Management Association*, 64, 1352-1360.
- 487
- 488 Ackermann, I.J., Hass, H., Memmesheimer, M., Ebel, A., Binkowski, F.S., Shankar, U., 1998. Modal aerosol dynamics
489 model for Europe: Development and first applications. *Atmospheric Environment*, 32, 17, 2981-2999.
- 490
- 491 Ahmadov, R., McKeen, S. A., Robinson, A. L., Bahreini, R., Middlebrook, A. M., de Gouw, J. A., Meagher, J., Hsie, E.-
492 Y., Edgerton, E., Shaw, S., Trainer, M., 2012. A volatility basis set model for summertime secondary organic aerosols
493 over the eastern United States in 2006. *J. Geophys. Res.*, 117, D06301.
- 494
- 495 Alapaty, K., Mathur, R., Pleim, J., Hogrefe, C., Rao, S.T., 2012. New Directions: Understanding interactions of air
496 quality and climate change at regional scales. *Atmospheric Environment*, 49, 419–421.
- 497
- 498 Baklanov, A., Schlünzen, K., Suppan, P., Baldasano, J., Brunner, D., Aksoyoglu, S., Carmichael, G., Douros, J.,
499 Flemming, J., Forkel, R., Galmarini, S., Gauss, M., Grell, G., Hirtl, M., Joffre, S., Jorba, O., Kaas, E., Kaasik, M.,
500 Kallos, G., Kong, X., Korsholm, U., Kurganskiy, A., Kushta, J., Lohmann, U., Mahura, A., Manders-Groot, A.,
501 Maurizi, A., Moussiopoulos, N., Rao, S. T., Savage, N., Seigneur, C., Sokhi, R. S., Solazzo, E., Solomos, S., Sørensen,
502 B., Tsegas, G., Vignati, E., Vogel, B., and Zhang, Y., 2014. Online coupled regional meteorology chemistry models in
503 Europe: current status and prospects. *Atmos. Chem. Phys.*, 14, 317-398.
- 504
- 505 Barnard J.C., Chapman, E.G., Fast, J., Schmelzer, J.R., Slusser, J.R., Shetter, R.E., 2004. An evaluation of the FAST-J
506 photolysis algorithm for predicting nitrogen dioxide photolysis rates under clear and cloudy sky conditions.
507 *Atmospheric Environment* 38, 3393–3403.
- 508
- 509 Barnard, J. C., Fast, J. D., Paredes-Miranda, G., Arnott, W. P., Laskin, A., 2010. Technical Note: Evaluation of the
510 WRF-Chem "Aerosol Chemical to Aerosol Optical Properties" Module using data from the MILAGRO campaign.
511 *Atmos. Chem. Phys.*, 10, 7325-7340.
- 512
- 513 Basart, S., Pay, M.T., Jorba, O., Pérez, C., Jiménez-Guerrero, P., Schulz, M., Baldasano, J.M., 2012. Aerosols in the
514 CALIOPE air quality modelling system: evaluation and analysis of PM levels, optical depths and chemical composition
515 over Europe. *Atmos. Chem. Phys.*, 12, 3363–3392.
- 516
- 517 Bianconi, R., Galmarini, S., Bellasio, R., 2004. Web-based system for decision support in case of emergency: ensemble
518 modelling of long-range atmospheric dispersion of radionuclides. *Environmental Modelling and Software* 19, 401-411.
- 519
- 520 Brunner, D., Eder, B., Jorba, O., Savage, N., Makar, P., Giordano, L., Badia, A., Balzarini, A., Baro, R., R., Chemel, C.,
521 Forkel, R., Jimenez-Guerrero, P., Hirtl, M., Hodzic, A., Honzak, L., Knote, C., Kuenen, J.J.P., Makar, P.A., Manders-
522 Groot, A., Davis, L., Perez, J.L., Pirovano, G., San Jose, R., Savage, N., Schroder, W., Sokhi, R.S., Syrakov, D., Torian,
523 A., Werhahn, K., Wolke, R., Yahya, K., Zabkar, R., Zhang, Y., Zhang, J., Hogrefe, C., Galmarini, S., 2014. Evaluation
524 of the meteorological performance of coupled chemistry-meteorology models in phase 2 of the Air Quality Model
525 Evaluation International Initiative. *Atmospheric Environment*, Submitted.
- 526
- 527 Byun, D. W., Ching, J. K. S., 1999. Science algorithms of the EPA Models-3 Community Multiscale Air Quality
528 (CMAQ) Modeling System. Report EPA-600/R-99/30, U.S. Environ. Prot. Agency, Washington, D.C.
- 529

- 530 Byun, D.W., Schere, K.L., 2006. Review of the Governing Equations, Computational Algorithms, and Other
531 Components of the Models-3 Community Multiscale Air Quality (CMAQ) Modeling System. *Applied Mechanics*
532 *Reviews*, 59, 2, 51-77.
533
- 534 Chapman, E. G., Gustafson Jr., W. I., Easter, R. C., Barnard, J. C., Ghan, S. J., Pekour, M. S., and Fast, J. D., 2009.
535 Coupling aerosol-cloud-radiative processes in the WRF-Chem model: Investigating the radiative impact of elevated
536 point sources. *Atmos. Chem. Phys.*, 9, 945-964.
537
- 538 Chen, F., Dudhia, J., 2001. Coupling an Advanced Land Surface-Hydrology Model with the Penn State-NCAR MM5
539 Modeling System. Part I: Model Implementation and Sensitivity. *Monthly Weather Review* 129, 569-585.
540
- 541 Cuvelier, C., Thunis, P., Vautard, R., Amann, M., Bessagnet, B., Bedogni, M., Berkowicz, R., Brandt, J., Brocheton, F.,
542 Builtjes, P., Carnevale, C., Copalle, A., Denby, B., Douros, J., Graf, A., Hellmuth, O., Honoré, C., Hodzic, A., Jonson,
543 J., Kerschbaumer, A., de Leeuw, F., Minguzzi, E., Moussiopoulos, N., Pertot, C., Peuch, V.H., Pirovano, G., Rouil, L.,
544 Sauter, F., Schaap, M., Stern, R., Tarrason, L., Vignati, E., Volta, M., White, L., Wind, P., Zuber, A., 2007. CityDelta:
545 A model intercomparison study to explore the impact of emission reductions in European cities in 2010. *Atmospheric*
546 *Environment* 41, issue 1, 189-207.
547
- 548 Eck, T.F., Holben, B.N., Reid, J.S., Dubovik, O., Smirnov, A., O'Neill, T.N., Slutsker, L., Kinne, S., 1999. Wavelength
549 dependence of the optical depth of biomass burning, urban, and desert dust aerosols. *J. Geophys. Res.*, 104, D24,
550 31,333-31,349.
551
- 552 DeMore, W. B., Sander, S. P., Golden, D. M., Hampson, R. F., Kurylo, M. J., Howard, C. J., Ravishankara, A. R., Kolb,
553 C. E., Molina, M. J., 1997. Chemical kinetics and photochemical data for use in stratospheric modeling, Eval. 12,
554 NASA, Jet Propul. Lab. Calif. Inst. of Technol., Pasadena.
555
- 556 Fast, J. D., Gustafson Jr., W. I., Easter, R. C., Zaveri, R. A., Barnard, J. C., Chapman, E. G., Grell, G. A., Peckham, S.
557 E., 2006. Evolution of ozone, particulates, and aerosol direct radiative forcing in the vicinity of Houston using a fully
558 coupled meteorology-chemistry-aerosol model. *J. Geophys. Res.*, 111, D21305.
559
- 560 Fahey, K. M., Pandis, S.N., 2001. Optimizing model performance: Variable size resolution in cloud chemistry
561 modeling. *Atmospheric Environment*, 35, 4471-4478.
562
- 563 Forkel, R., Balzarini, A., Baró, R., Curci, G., Jiménez-Guerrero, P., Hirtl, M., Honzak, L., Im, U., Lorenz, C., Pérez,
564 J.L., Pirovano, G., San José, R., Tuccella, P., Werhahn, J., Žabkar, R., 2014. Analysis of the WRF-Chem contributions
565 to AQMEII phase2 with respect to aerosol radiative feedbacks on meteorology and pollutant distribution. *Atmospheric*
566 *Environment*, Submitted.
567
- 568 Galmarini, S., Bianconi, R., Appel, W., Solazzo, E., et al., 2012. ENSEMBLE and AMET: two systems and approaches
569 to a harmonised, simplified and efficient assistance to air quality model developments and evaluation. *Atmospheric*
570 *Environment*, 53, 51-59.
571
- 572 Gery, M. W., Whitten, G. Z., Killus, J. P., Dodge, M. C., 1989. A photochemical kinetics mechanism for urban and
573 regional scale computer modeling. *J. Geophys. Res.*, 94, 12,925-12,956.
574
- 575 Ghan, S., Laulainen, N., Easter, R., Wagener, R., Nemesure, S., Chapman, E., Zhang, Y., and Leung, R., 2001.
576 Evaluation of aerosol direct radiative forcing in MIRAGE. *J. Geophys. Res.*, 106, 5295-5316.
577
- 578 Gong, S. L., 2003. A parameterization of sea-salt aerosol source function for sub- and super-micron particles. *Global*
579 *Biogeochemical Cycles* 17, 1097-1104.
580
- 581 Grell, G. A., Devenyi, D., 2002. A generalized approach to parameterizing convection combining ensemble and data
582 assimilation techniques. *Geophys. Res. Lett.* 29, 14, 1693.
583

- 584 Grell, G. A., Peckham, S. E., Schmitz, R., McKeen, S. A., Frost, G., Skamarock, W. C., and Eder, B., 2005. Fully
585 coupled online chemistry within the WRF model. *Atmos. Environ.*, 39, 6957–6975.
586
- 587 Grell, G., Baklanov, A., 2011. Coupled Modeling for Forecasting Weather and Air Quality. *Atmospheric Environment*,
588 45, 38, 6845–6851.
589
- 590 Grell, G.A., Freitas, S.R., 2014. A scale and aerosol aware stochastic convective parameterization for
591 weather and air quality modeling. *Atmos. Chem. Phys.*, 14, 5233–5250.
592
- 593 Guenther A., Karl T., Harley P., Wiedinmyer C., Palmer P.I., and Geron C., 2006. Estimates of global terrestrial
594 isoprene emissions using MEGAN (Model of Emissions of Gases and Aerosols from Nature. *Atmospheric Chemistry
595 and Physics*, 6, 3181-3210.
596
- 597 Hong, S.-Y., Noh, Y., Dudhia, J., 2006. A New Vertical Diffusion Package with an Explicit Treatment of Entrainment
598 Processes. *Monthly Weather Review* 134, 2318-2341.
599
- 600 Iacono, M. J., J. S. Delamere, E. J. Mlawer, M. W. Shephard, S. A. Clough, and W. D. Collins, 2008. Radiative forcing
601 by long-lived greenhouse gases: Calculations with the AER radiative transfer models. *J. Geophys. Res.*, 113, D13103.
602
- 603 Im, U., Bianconi, R., Solazzo, E., Kioutsioukis, I., Badia, A., Balzarini, A., Baró, R., Bellasio, R., Brunner, D., Chemel,
604 C., Curci, G., Denier van der Gon, H., Flemming, J., Forkel, R., Giordano, L., Jiménez-Guerrero, P., Hirtl, M., Hodzic,
605 A., Honzak, L., Jorba, O., Knote, C., Makar, P.A., Manders-Groot, A., Neal, L., Pérez, J.L., Pirovano, G., Pouliot, G.,
606 San Jose, R., Savage, N., Schroder, W., Sokhi, R.S., Syrakov, D., Torian, A., Tuccella, P., Wang, K., Werhahn, J.,
607 Wolke, R., Zabkar, R., , Zhang, Y., Zhang, J., Hogrefe, C., Galmarini, S., 2014. Evaluation of operational online-
608 coupled regional air quality models over Europe and North America in the context of AQMEII phase2. Part II:
609 Particulate Matter. *Atmospheric Environment*, this issue, doi: 10.1016/j.atmosenv.2014.08.072.
610
- 611 Kallos, G., Astitha, M., Katsafados, P., Spyrou, C., 2007. Long-range transport of anthropogenically and naturally
612 produced particulate matter in the Mediterranean and North Atlantic: current status of knowledge. *J. Appl. Meteorol.*
613 *Climatol.* 46, 1230-1251.
614
- 615 Kondragunta, S., Lee, P., McQueen, J., Kittaka, C., Ciren, P., Prados, A., Laszlo, I., Pierce, R. B., Hoff, R., Szykman,
616 J.J., 2008. Air quality forecast verification using satellite data. *J. Appl. Meteorol.*, 47, 443– 461.
617
- 618 Kuenen, J.J.P., Visschedijk, A.J.H., Jozwicka, M., Denier van der Gon, H.A.C., 2014. TNO_MACC_II emission
619 inventory: a multi-year (2003-2009) consistent high-resolution European emission inventory for air quality modelling.
620 *Atmospheric Chemistry and Physics Discussions*, 14, 5837-5869.
621
- 622 McKeen, S., Chung, S. H., Wilczak, J., Grell, G., Djalalova, I., Peckham, S., Gong, W., Bouchet, V., Moffet, R.,
623 Tang, Y., Carmichael, G. R., Mathur, R., Yu, S., 2007. Evaluation of several PM_{2.5} forecast models using data
624 collected during the ICARTT/NEAQS 2004 field study. *J. Geophys. Res.*, 112, D10S20.
625
- 626 Middleton, P., Stockwell, W. R., Carter, W. P., 1990. Aggregation and analysis of volatile organic compound emissions
627 for regional modelling. *Atmos. Environ.*, 24, 1107–1133.
628
- 629 Mitsakou, C., Kallos, G., Papantoniou, N., Spyrou, C., Solomos, S., Astitha, M., Housiadas, C., 2008. Saharan dust
630 levels in Greece and received inhalation doses. *Atmos. Chem. Phys.* 8, 7181-7192.
631
- 632 Morrison, H., Thompson, G., Tatarskii, V, 2009. Impact of cloud microphysics on the development of trailing stratiform
633 precipitation in a simulated squall line: Comparison of one- and two-moment schemes. *Monthly Weather Review* 137,
634 991-1007.
635
- 636 Mozurkewich, M., 1993. The dissociation constant of ammonium nitrate and its dependence on temperature, relative
637 humidity and particle size. *Atmospheric Environment* 27A, 261-270.

638

639 Papadimas, C. D., Hatzianastassiou, N., Mihalopoulos, N., Querol, X., Vardavas, I., 2008. Spatial and temporal
640 variability in aerosol properties over the Mediterranean basin based on 6-year (2000–2006) MODIS data. *J. Geophys.*
641 *Res.*, 113, D11205.

642

643 Pernigotti, D., Thunis, P., Cuvelier, C., Georgieva, E., Gsella, A., De Meij, A., Pirovano, G., Balzarini, A., Riva, G.M.,
644 Carnevale, C., Pisoni, E., Volta, M., Bessagnet, B., Kerschbaumer, A., Viaene, P., De Ridder, K., Nyiri, A., Wind, P.,
645 2013. POMI: a model inter-comparison exercise over the Po Valley. *Air Qual Atmos Health* 6(4), 701-715.

646

647 Pirovano, G., Balzarini, A., Bessagnet, B., Emery, C., Kallos, G., Meleux, F., Mitsakou, C., Nopmongcol, U., Riva,
648 G.M., Yarwood, G., 2012. Investigating impacts of chemistry and transport model formulation on model performance at
649 European scale. *Atmospheric Environment* 53, 93-109.

650

651 Pouliot, G., Pierce, T., Denier van der Gon, H., Schaap, M., Moran, M., Nopmongcol, U., 2012. Comparing emissions
652 inventories and model-ready emissions datasets between Europe and North America for the AQMEII Project.
653 *Atmospheric Environment* 53, 75-92.

654

655 Pouliot, G., Denier van der Gon, H., Kuenen, J., Makar, P., Zhang, J., Moran, M., 2014. Analysis of the Emission
656 Inventories and Model-Ready Emission Datasets of Europe and North America for Phase 2 of the AQMEII Project.
657 *Atmospheric Environment*, Submitted.

658

659 Rao, S. T., Galmarini, S., Puckett, K., 2011. Air Quality Model Evaluation International Initiative (AQMEII):
660 Advancing the State of the Science in Regional Photochemical Modeling and Its Applications. *BAMS*, Volume 92,
661 Issue 1, 23-30.

662

663 Robles González, C., Schaap, M., de Leeuw, G., Builtjes, P.J.H., van Loon, M., 2003. Spatial variation of aerosol
664 properties over Europe derived from satellite observation and comparison with model calculations. *Atmos. Chem.*
665 *Phys.*, 3, 521-533.

666

667 Roy, B., Mathur, R., Gilliland, A.B., Howard, S.C., 2007. A comparison of CMAQ-based aerosol properties with
668 IMPROVE, MODIS, and AERONET data. *J. Geophys. Res.*, 112, D14301.

669

670 San José, R., Pérez, J.L., Balzarini, A., Baró, R., Curci, G., Forkel, R., Galmarini, S., Grell, G., Hirtl, M., Honzak, L.,
671 Im, U., Jiménez-Guerrero, P., Langer, M., Pirovano, G., Tuccella, P., Werhahn, J., Žabkar, R., 2014. Evaluation of
672 feedback effects in CBMZ/MOSAIC chemical mechanism. *Atmospheric Environment*, Submitted.

673

674 Schell, B., Ackermann, I.J., Hass, H., Binkowski, F.S., Ebel, A., 2001. Modeling the formation of secondary organic
675 aerosol within a comprehensive air quality model system, *Journal of Geophysical Research*, 106, 28275-28293.

676

677 Seinfeld, J.H., and S.N. Pandis. 1998. *Atmospheric Chemistry and Physics, From Air Pollution to Climate Change*.
678 John Wiley and Sons, Inc., NY.

679

680 Shaw, W.J., Allwine, K., Fritz, B.G., Rutz, F.C., Rishel, J.P., Chapman, E.G., 2008. An evaluation of the wind erosion
681 module in DUSTRAN. *Atmospheric Environment* 42, 1907–1921.

682

683 Skamarock, W. C. and Klemp, J. B., 2008. A time-split nonhydrostatic atmospheric model for research and NWP
684 applications. *J. Comput. Phys.*, 227, 3465–3485.

685

686 Solazzo, E., Bianconi, R., Vautard, R., Appel, K.W., Moran, M.D., Hogrefe, C., et al., 2012. Model evaluation and
687 ensemble modelling of surface-level ozone in Europe and North America in the context of AQMEII. *Atmospheric*
688 *Environment* 53, 60-74.

689

690 Stockwell, W. R., P. Middleton, J. S. Chang, and X. Tang, 1990. The second generation regional acid deposition model
691 chemical mechanism for regional air quality modeling. *J. Geophys. Res.*, 95, 16343-16367.

692

693 Tombette, M., Chazette, P., Sportisse, B., and Roustan, Y.: Simulation of aerosol optical properties over Europe with a
694 3-D size-resolved aerosol model: comparisons with AERONET data, *Atmos. Chem. Phys.*, 8, 7115-7132,
695 doi:10.5194/acp-8-7115-2008, 2008.

696

697 Tuccella, P., G. Curci, G. Visconti, B. Bessagnet, L. Menut, and R. J. Park, 2012. Modeling of gas and aerosol with
698 WRF/Chem over Europe: Evaluation and sensitivity study. *J. Geophys. Res.*, 117, D03303.

699

700 Van Loon, M., Vautard, R., Schaap, M., Bergstrom, R., Bessagnet, B., Brandt, J., Bultjes, P., Christensen, J.H.,
701 Cuvelier, K., Graf, A., Jonson, J., Krol, M., Langner, J., Roberts, P., Rouil, L., Stern, R., Tarrason, L., Thunis, P.,
702 Vignati, E., White, L., Wind, P, 2007. Evaluation of long-term ozone simulations from seven regional air quality
703 models and their ensemble average. *Atmos. Environ.* 41, 2083–2097.

704

705 Walcek and Taylor, 1986. A theoretical Method for computing vertical distributions of acidity and sulfate within
706 cumulus clouds. *J. Atmos Sci.*, 43, 4, 339 – 355.

707

708 Wesely M.L, 1989. Parameterization of surface resistance to gaseous dry deposition in regional-scale numerical models.
709 *Atmos. Environ.*, 23, 1293-1304.

710

711

712 Yarwood, G., Rao, S., Yocke, M., Whitten, G. Z., 2005. Final Report-Updates to the Carbon Bond Chemical
713 Mechanism: CB05. Rep. RT-04-00675, 246 pp., Yocke and Co., Novato, California [Available at
714 http://www.camx.com/publ/pdfs/CB05_Final_Report_120805.pdf].

715

716 Zaveri, R.A., Peters, L.K., 1999. A new lumped structure photochemical mechanism for large-scale applications. *J.*
717 *Geophys. Research*, 104, D23, 30,387-30,415.

718

719 Zaveri, R., Easter, R.C., Fast, J.D., Peters, L.K., 2008. Model for Simulating Aerosol Interactions and Chemistry
720 (MOSAIC). *Journal of Geophysical Research*, 113, D13204.

721

722 Zhao, C., Liu, X., Leung, L. R., Johnson, B, McFarlane, S. A., Gustafson Jr., W. I., Fast, J.D., Easter, R., 2010. The
723 spatial distribution of mineral dust and its shortwave radiative forcing over North Africa: modeling sensitivities to dust
724 emissions and aerosol size treatments. *Atmos. Chem. Phys.*, 10, 8821–8838.

725

726 Zhang, Y., Chen, Y., Sarwar, G., Schere, K., 2012. Impact of gas-phase mechanisms on Weather Research
727 Forecasting Model with Chemistry (WRF/Chem) predictions: Mechanism implementation and comparative evaluation.
728 *J. Geophys. Res.*, 117, D01301.

729

730 Zhang, Y., Wen, X.-Y., and Jang, C. J., 2010. Simulating chemistry–aerosol–cloud–radiation–climate feedbacks over
731 the continental US using the online-coupled Weather Research Forecasting Model with chemistry (WRF/Chem).
732 *Atmos. Environ.*, 44, 3568-3582.

733

Table 1: Statistical performances of IT1 and SI2 simulation for gaseous and aerosol compounds over the whole European domain.

	Observed		IT1			SI2			PCC
	Mean ($\mu\text{g}/\text{m}^3$)	Mean ($\mu\text{g}/\text{m}^3$)	NMB (%)	RMSE ($\mu\text{g}/\text{m}^3$)	PCC	Mean ($\mu\text{g}/\text{m}^3$)	NMB (%)	RMSE ($\mu\text{g}/\text{m}^3$)	
gas compounds									
O ₃	39.58	31.04	-12.32	11.32	0.82	36.92	-3.75	8.42	0.85
SO ₂	4.78	2.79	-41.64	6.49	0.44	2.63	-45.62	6.53	0.46
NO ₂	18.88	11.94	-36.74	14.94	0.54	11.35	-39.88	15.26	0.54
aerosol compounds									
PM10	20.01	14.84	-25.82	16.60	0.38	15.42	-22.94	16.85	0.35
PM2.5	13.73	11.80	-14.05	12.58	0.42	12.12	-11.76	12.68	0.42
SO ₄	1.79	0.95	-47.02	1.95	0.48	2.16	20.67	1.95	0.48
NO ₃	1.81	3.35	85.19	3.27	0.57	4.00	110.86	4.00	0.60
NH ₄	0.86	1.13	31.84	1.10	0.59	1.85	114.82	1.76	0.56

Table 2: Statistical performances of IT1 and SI2 simulation for aerosol optical depth at the wavelength of 555nm at each European station. Performances are also reported for the whole pool of stations.

	Observed	IT1				SI2			
	Mean	Mean	NMB (%)	RMSE	PCC	Mean	NMB (%)	RMSE	PCC
Burjassot	0.12	0.09	-25.73	0.09	0.55	0.12	-1.20	0.10	0.56
Caceres	0.11	0.09	-22.89	0.09	0.50	0.10	-13.01	0.10	0.52
Carpentras	0.11	0.10	-14.42	0.10	0.36	0.11	0.70	0.09	0.47
Crete	0.17	0.14	-16.24	0.11	0.38	0.17	0.36	0.11	0.47
Cyprus	0.20	0.14	-30.03	0.14	0.48	0.15	-24.85	0.13	0.49
Evora	0.10	0.10	3.19	0.10	0.43	0.11	9.04	0.10	0.46
Granada	0.12	0.09	-23.63	0.09	0.52	0.10	-14.66	0.08	0.60
Lampedusa	0.16	0.14	-9.35	0.13	0.60	0.18	13.08	0.15	0.53
Lecce University	0.15	0.11	-26.05	0.11	0.34	0.15	1.75	0.10	0.52
Malaga	0.15	0.12	-21.02	0.09	0.61	0.16	5.92	0.12	0.60
Nes Ziona	0.25	0.16	-37.61	0.20	0.49	0.17	-31.79	0.18	0.55
Sevastopol	0.17	0.15	-15.05	0.11	0.42	0.18	7.19	0.11	0.47
All Stations	0.15	0.12	-21.49	0.12	0.51	0.14	-6.39	0.12	0.52

Figure Captions

Figure 1: AQMEII computational domain.

Figure 2: O₃ (a), NO₂ (b), SO₂ (c), H₂O₂ (d) and HNO₃ (e) yearly mean concentrations at the ground for IT1 (left), SI2 (center) simulation and the difference between IT1 and SI2 (right).

Figure 3: O₃ (a), NO₂ (b) and SO₂ (c) time series of daily mean concentrations (right) and box whisker plots of hourly data (left) for the year 2010. Time series data are reported as mean concentrations of all available measurement stations for each compound.

Figure 4: PM10 (a) and PM2.5 (b) yearly mean concentrations at the ground for IT1 (left), SI2 (center) simulation and the difference between IT1 and SI2 (right).

Figure 5: fine SO₄ (a), NO₃ (b), NH₄ (c) elemental carbon (d) and organic carbon (e) yearly mean concentrations at the ground for IT1 (left), SI2 (center) simulation and the difference between IT1 and SI2 (right).

Figure 6: SO₄ (a), NO₃ (b) and NH₄ (c) time series of daily mean concentrations (right) and box whisker plots (left) for the year 2010. Time series data are reported as mean concentrations of all available measurement stations for each compound.

Figure 7: yearly mean of Aerosol Optical Depth at 555 nm wavelength (AOD555) for IT1 (left) and SI2 (center) simulation and the difference between IT1 and SI2 (right). Circles indicate the observed yearly mean AODs at each AERONET station.

Figure 8: Aerosol Optical Depth at 555 nm wavelength (AOD555) time series of daily mean values at all AERONET stations (right) and box whisker plots (left) for the year 2010.

Figure 9: Aerosol Optical Depth at 555 nm wavelength (AOD555) time series of daily mean values at Lampedusa (a) and Malaga (b) AERONET stations.

Figure 10: Scatter plot diagram of Aerosol Optical Depth at 555 nm wavelength (AOD555) daily differences versus NO₃ (left) and SO₄ (right) daily differences at Lampedusa (a) and Malaga (b) AERONET stations for the year 2010. Differences are calculated as IT1 - SI2.

Figure 11: Aerosol Optical Depth at 555 nm wavelength (AOD555) time series of daily mean values at Cyprus (a) and Ness Ziona (b) AERONET stations for the year 2010.

Figure 12: Scatter plot diagram of Aerosol Optical Depth at 555 nm wavelength (AOD555) daily biases versus daily Angstrom exponent at Cyprus (a) and Ness Ziona (b) AERONET stations for the year 2010.

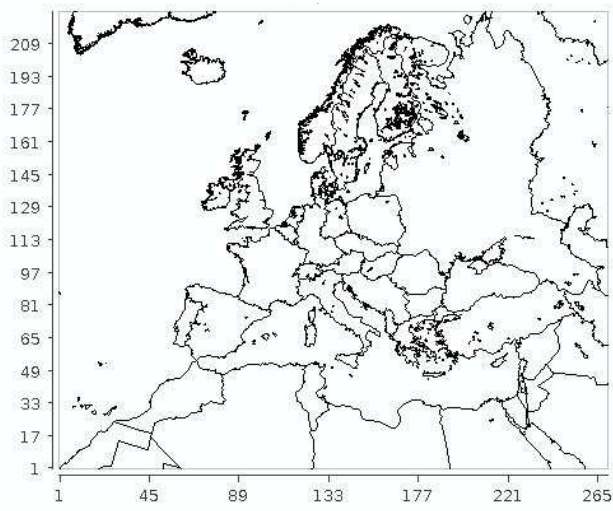


Figure 1: AQMEII computational domain.

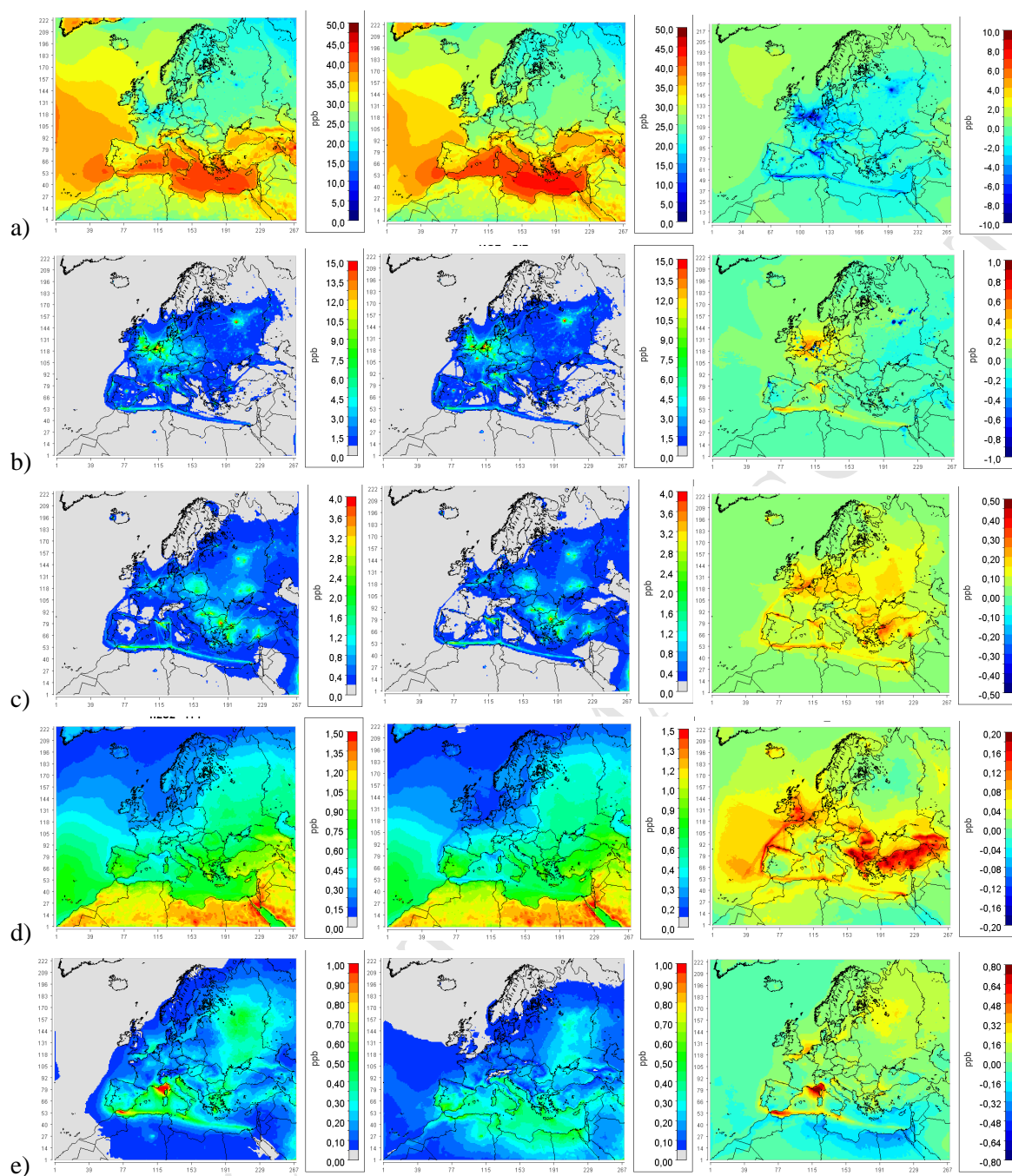


Figure 2: O_3 (a), NO_2 (b), SO_2 (c), H_2O_2 (d) and HNO_3 (e) yearly mean concentrations at the ground for IT1 (left), SI2 (center) simulation and the difference between IT1 and SI2 (right).

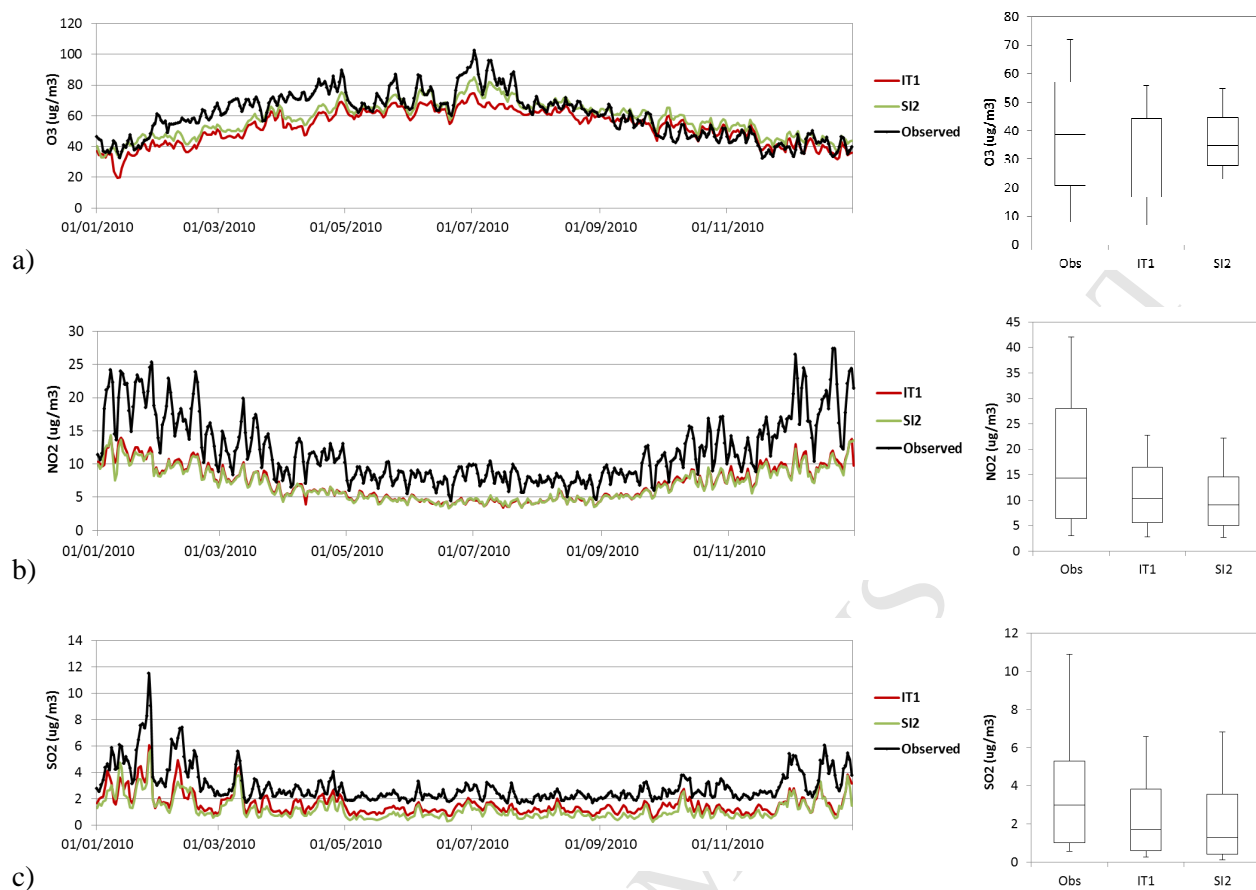


Figure 3: O₃ (a), NO₂ (b) and SO₂ (c) time series of daily mean concentrations (right) and box whisker plots of hourly data (left) for the year 2010. Time series data are reported as mean concentrations of all available measurement stations for each compound.

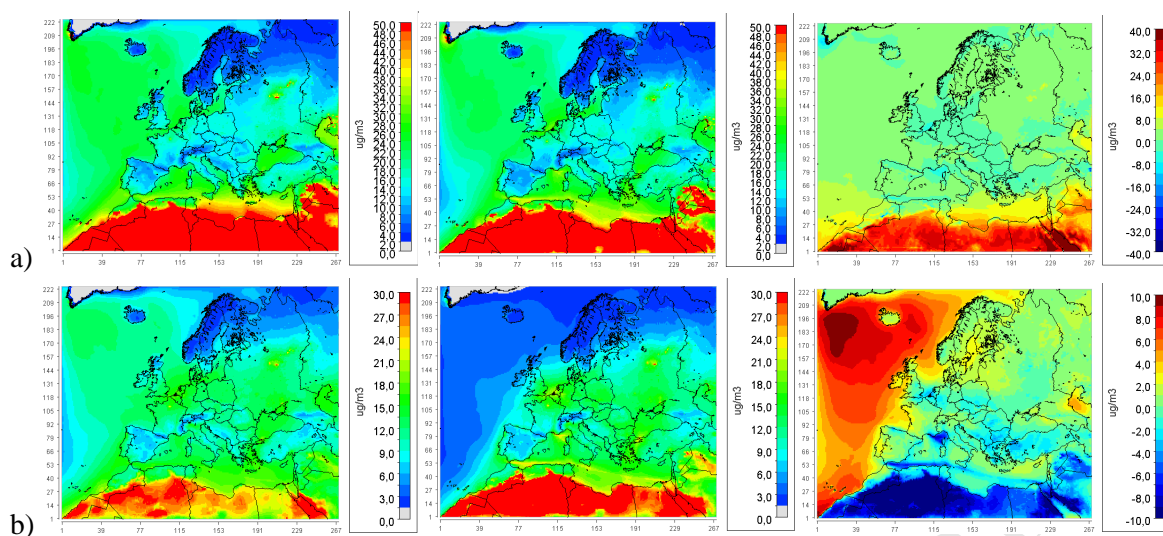


Figure 4: PM10 (a) and PM2.5 (b) yearly mean concentrations at the ground for IT1 (left), SI2 (center) simulation and the difference between IT1 and SI2 (right).

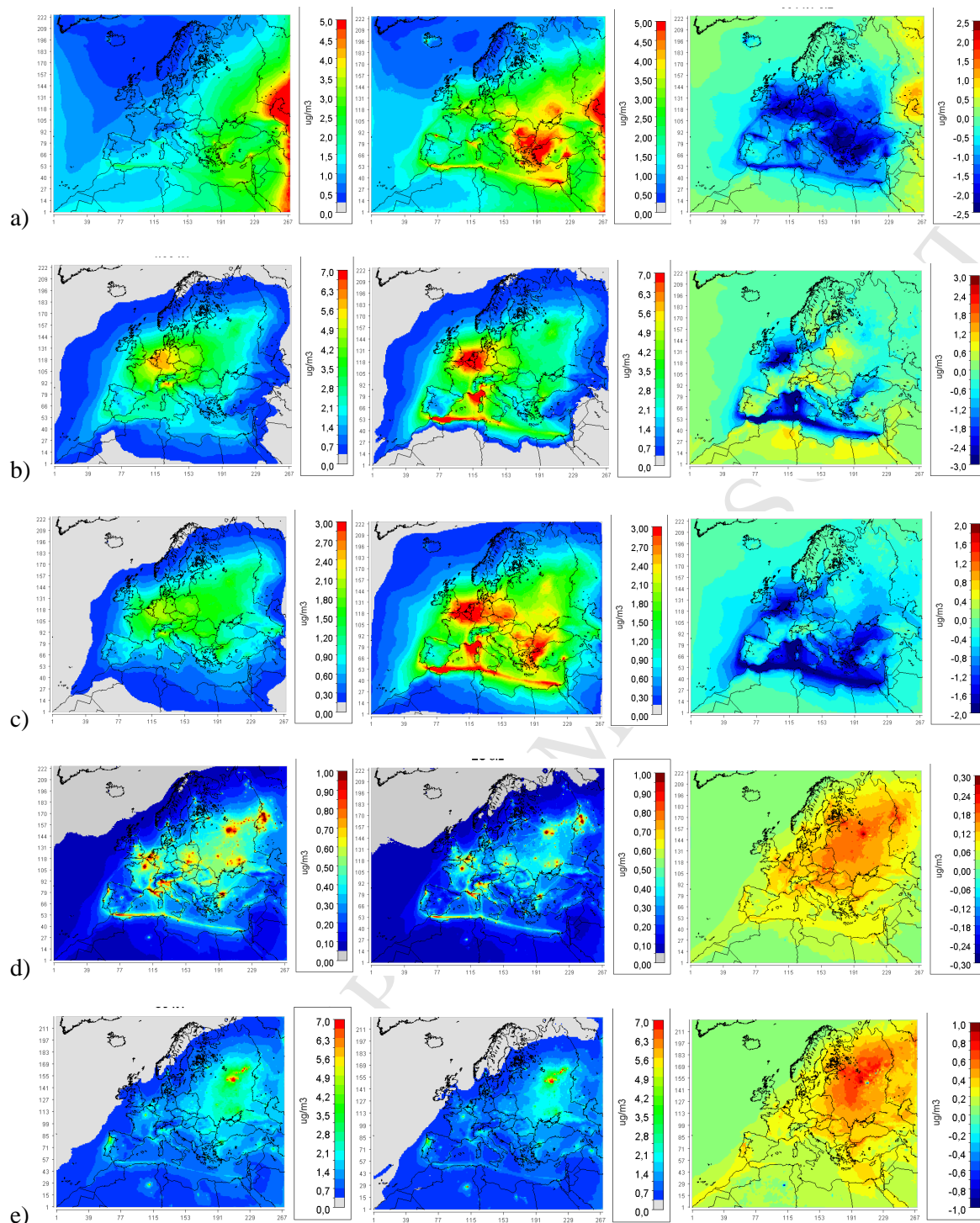


Figure 5: fine SO₄ (a), NO₃ (b), NH₄ (c) elemental carbon (d) and organic carbon (e) yearly mean concentrations at the ground for IT1 (left), SI2 (center) simulation and the difference between IT1 and SI2 (right).

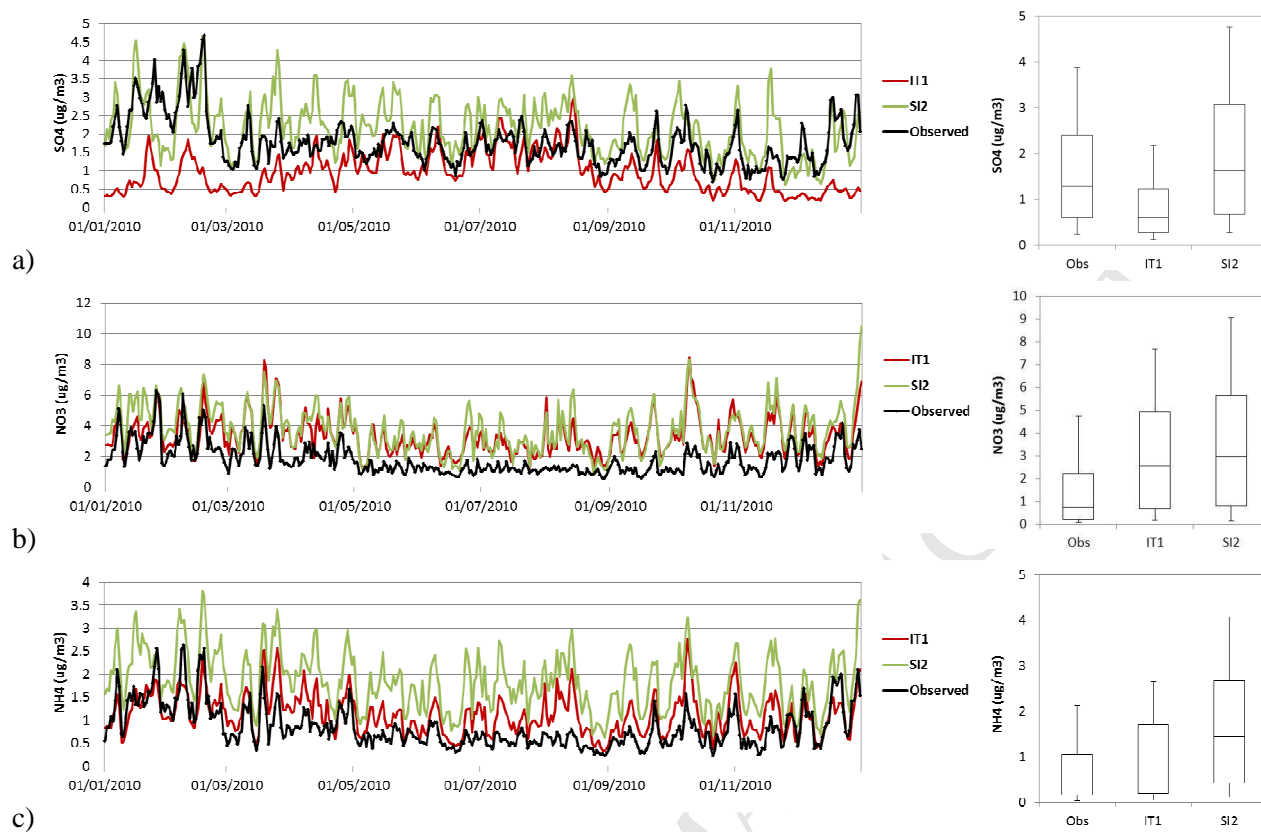


Figure 6: SO₄ (a), NO₃ (b) and NH₄ (c) time series of daily mean concentrations (right) and box whisker plots (left) for the year 2010. Time series data are reported as mean concentrations of all available measurement stations for each compound.

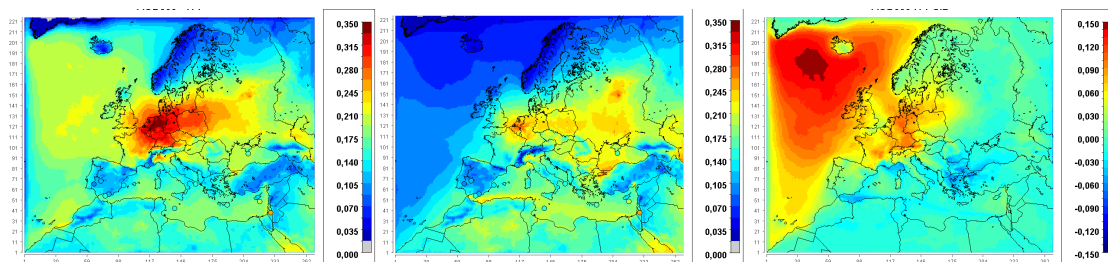


Figure 7: yearly mean of Aerosol Optical Depth at 555 nm wavelength (AOD555) for IT1 (left) and SI2 (center) simulation and the difference between IT1 and SI2 (right). Circles indicate the observed yearly mean AODs at each AERONET station.

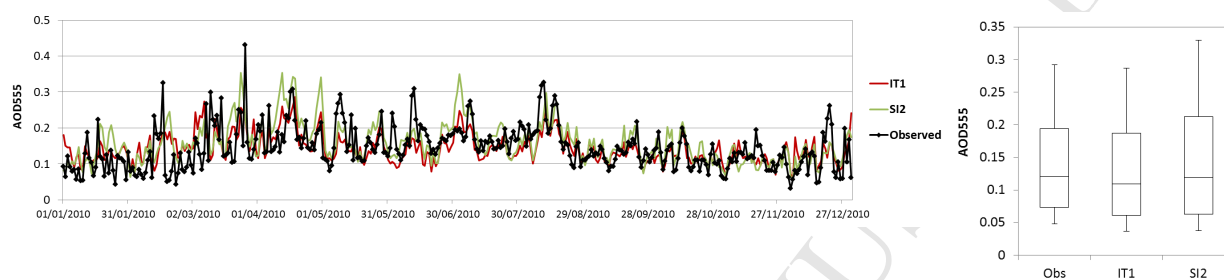


Figure 8: Aerosol Optical Depth at 555 nm wavelength (AOD555) time series of daily mean values at all AERONET stations (right) and box whisker plots (left) for the year 2010.

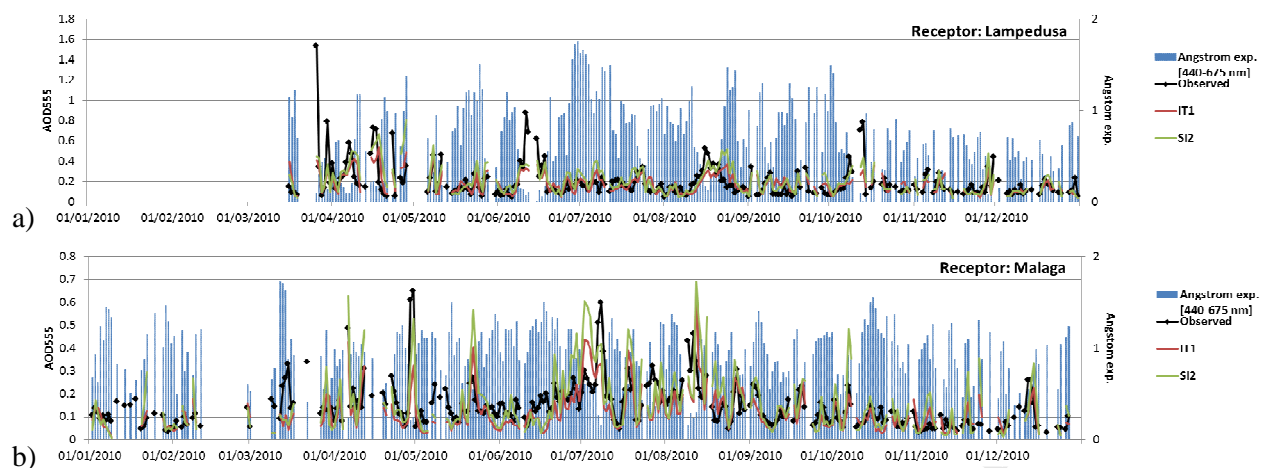


Figure 9: Aerosol Optical Depth at 555 nm wavelength (AOD555) time series of daily mean values at Lampedusa (a) and Malaga (b) AERONET stations.

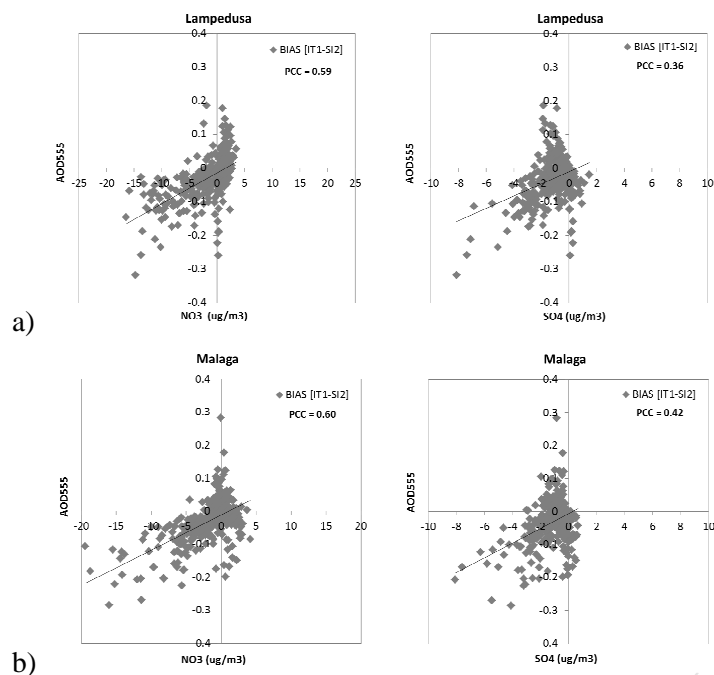


Figure 10: Scatter plot diagram of Aerosol Optical Depth at 555 nm wavelength (AOD555) daily differences versus NO₃ (left) and SO₄ (right) daily differences at Lampedusa (a) and Malaga (b) AERONET stations for the year 2010. Differences are calculated as IT1 - SI2.

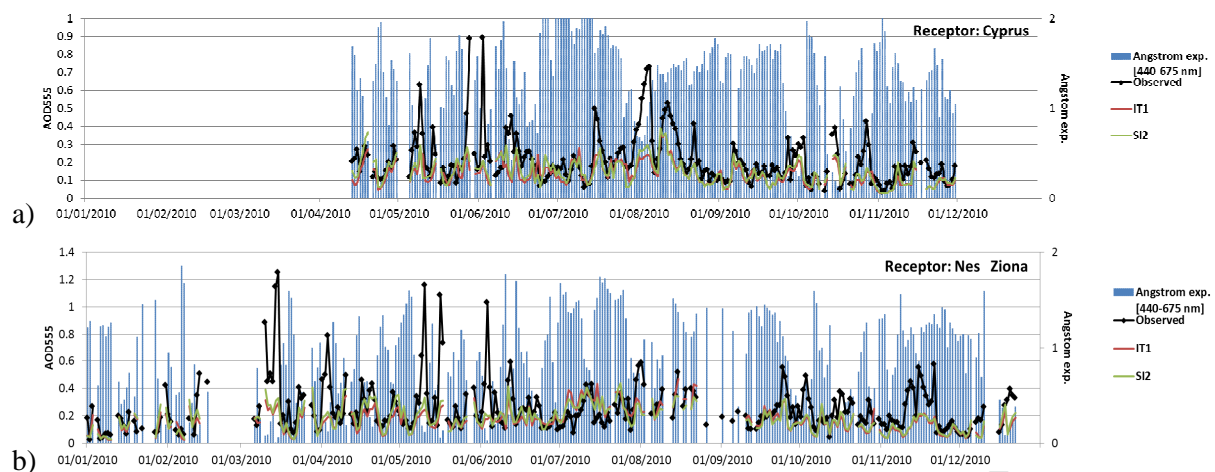
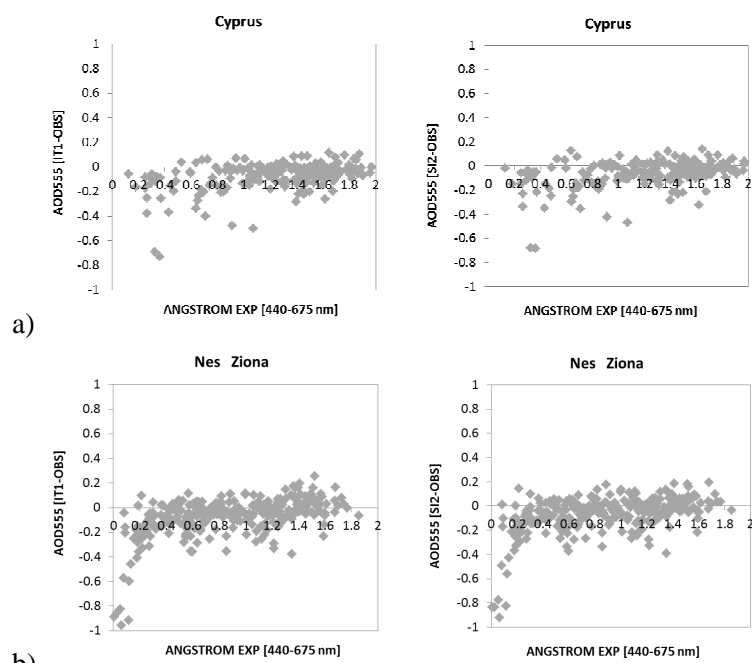


Figure 11: Aerosol Optical Depth at 555 nm wavelength (AOD555) time series of daily mean values at Cyprus (a) and Nes Ziona (b) AERONET stations for the year 2010.



b)

Figure 12: Scatter plot diagram of Aerosol Optical Depth at 555 nm wavelength (AOD555) daily biases versus daily Angstrom exponent at Cyprus (a) and Nes Ziona (b) AERONET stations for the year 2010.

Table S1: Geographical characteristics of AERONET stations included in the analysis.

Station	Longitude	Latitude	Elevation (m asl)	Data availability (%)
Burjassot	-0.42	39.51	30	24.51
Caceres	-6.34	39.48	397	21.39
Carpentras	5.06	44.08	100	22.27
Crete	25.28	35.33	20	24.69
Cyprus	33.04	34.68	22	24.73
Evora	-7.91	38.57	293	24.50
Granada	-3.61	37.16	680	25.53
Lampedusa	12.63	35.52	45	20.21
Lecce University	18.11	40.34	30	21.16
Malaga	-4.48	36.72	40	26.38
Ness Ziona	34.79	31.92	40	24.82
Sevastopol	33.52	44.62	80	22.64

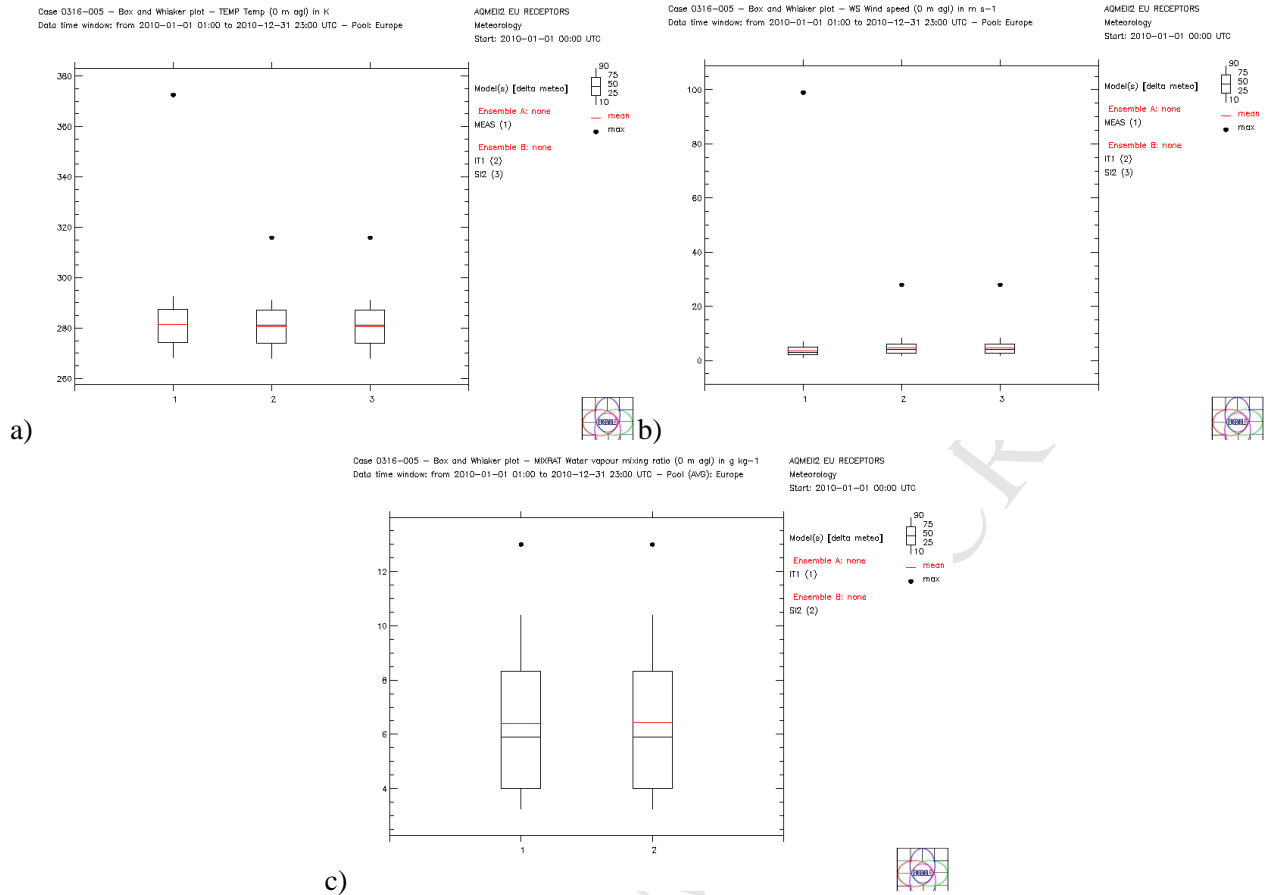


Figure S1: Temperature (a), wind speed (b) and mixing ratio(c) yearly box whisker plots of IT1 and SI2 simulations. SYNOP (surface synoptic observations) stations of the World Meteorological Organization (WMO) are compared to model results only for temperature and wind speed.

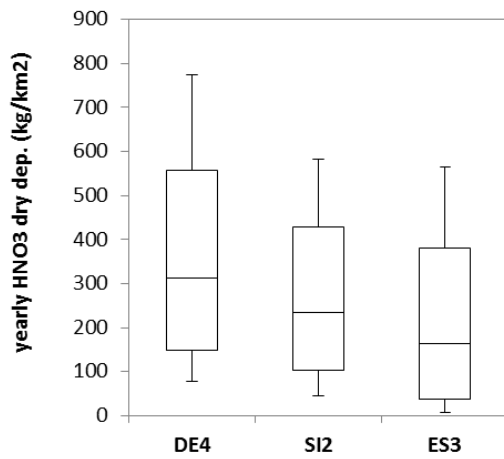


Figure S2: yearly HNO₃ dry deposition box whisker plots of DE4, SI2 and ES3 simulations. DE4 and ES3 configuration are described in Forkel et al. (2014) and San Josè et al. (2014), respectively.

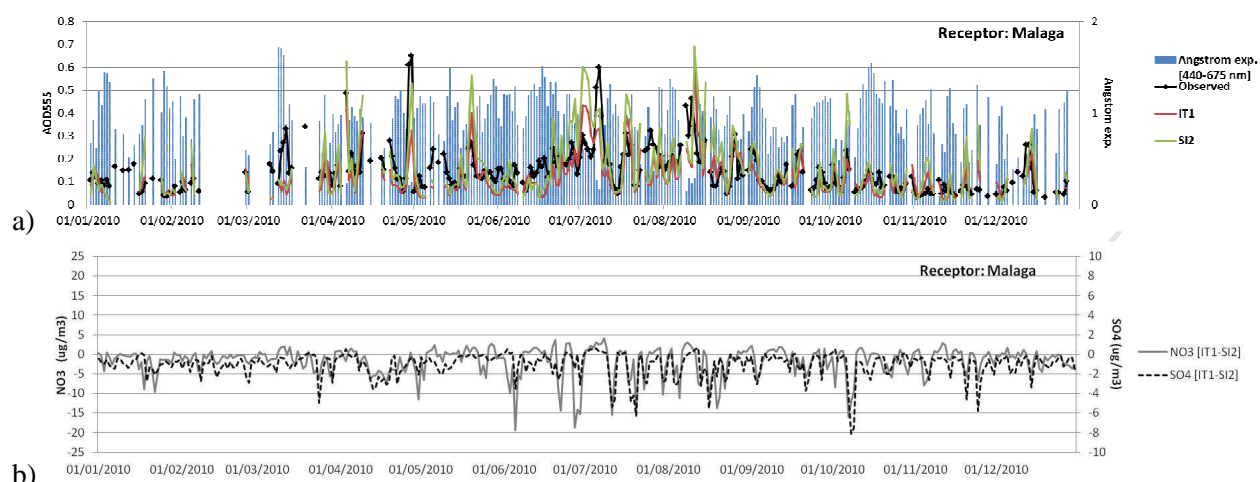


Figure S3: Aerosol Optical Depth (AOD555) time series of daily mean values at Malaga AERONET stations. Differences between IT1 and SI2 are also reported for sulfate and nitrate for the year 2010.